NASA/TM—2018-219911

Axial-Flow Turbine Rotor Discharge-Flow Overexpansion and Limit-Loading Condition

Part 2: Method of Analysis and Performance Evaluation of Computer Code AXOD2

Shu-Cheng S. Chen
Glenn Research Center, Cleveland, Ohio

June 2018

NASA STI Program . . . in Profile

Since its founding, NASA has been dedicated to the advancement of aeronautics and space science. The NASA Scientific and Technical Information (STI) Program plays a key part in helping NASA maintain this important role.

The NASA STI Program operates under the auspices of the Agency Chief Information Officer. It collects, organizes, provides for archiving, and disseminates NASA's STI. The NASA STI Program provides access to the NASA Technical Report Server—Registered (NTRS Reg) and NASA Technical Report Server—Public (NTRS) thus providing one of the largest collections of aeronautical and space science STI in the world. Results are published in both non-NASA channels and by NASA in the NASA STI Report Series, which includes the following report types:

- TECHNICAL PUBLICATION. Reports of completed research or a major significant phase of research that present the results of NASA programs and include extensive data or theoretical analysis. Includes compilations of significant scientific and technical data and information deemed to be of continuing reference value. NASA counter-part of peer-reviewed formal professional papers, but has less stringent limitations on manuscript length and extent of graphic presentations.

- TECHNICAL MEMORANDUM. Scientific and technical findings that are preliminary or of specialized interest, e.g., "quick-release" reports, working papers, and bibliographies that contain minimal annotation. Does not contain extensive analysis.

- CONTRACTOR REPORT. Scientific and technical findings by NASA-sponsored contractors and grantees.

- CONFERENCE PUBLICATION. Collected papers from scientific and technical conferences, symposia, seminars, or other meetings sponsored or co-sponsored by NASA.

- SPECIAL PUBLICATION. Scientific, technical, or historical information from NASA programs, projects, and missions, often concerned with subjects having substantial public interest.

- TECHNICAL TRANSLATION. English-language translations of foreign scientific and technical material pertinent to NASA's mission.

For more information about the NASA STI program, see the following:

- Access the NASA STI program home page at http://www.sti.nasa.gov

- E-mail your question to help@sti.nasa.gov

- Fax your question to the NASA STI Information Desk at 757-864-6500

- Telephone the NASA STI Information Desk at 757-864-9658

- Write to:
  NASA STI Program
  Mail Stop 148
  NASA Langley Research Center
  Hampton, VA 23681-2199

NASA/TM—2018-219911

Axial-Flow Turbine Rotor Discharge-Flow Overexpansion and Limit-Loading Condition

Part 2: Method of Analysis and Performance Evaluation of Computer Code AXOD2

Shu-Cheng S. Chen
Glenn Research Center, Cleveland, Ohio

National Aeronautics and
Space Administration

Glenn Research Center
Cleveland, Ohio 44135

June 2018

This work was sponsored by the Advanced Air Vehicle Program
at the NASA Glenn Research Center

Level of Review: This material has been technically reviewed by technical management.

Available from

NASA STI Program
Mail Stop 148
NASA Langley Research Center
Hampton, VA 23681-2199

National Technical Information Service
5285 Port Royal Road
Springfield, VA 22161
703-605-6000

This report is available in electronic form at http://www.sti.nasa.gov/ and http://ntrs.nasa.gov/

Contents

Axial-Flow Turbine Rotor Discharge-Flow Overexpansion and Limit-Loading Condition
Part 2: Method of Analysis and Performance Evaluation of Computer Code AXOD2

Shu-Cheng S. Chen
National Aeronautics and Space Administration
Glenn Research Center
Cleveland, Ohio 44135

Summary

The supercritical flow model-treatment implemented in AXOD2 is unique of its kind, and unique to axial-flow turbines. It is a rather simple, one-dimensional modeling concept which utilizes and captures two supercritical flow characteristics:

1. The mass flow rate remains to be a constant in supercritical flow conditions.
2. The flow angle at the choked blade-row-discharge deflects against the blade angle.

The two characteristics are linked mathematically, they are co-dependent in the model treatment of AXOD2. The treatment is highly analytical, follows mathematical principles and fundamental laws of gas dynamics rigorously. The mathematics and formulation applied to the supercritical flow treatment of AXOD2 are described and presented thoroughly in this paper, as they have not been revealed as clearly before. The head-to-head, quantitative comparison of the performance of AXOD2 to experimental data obtained in a rotating turbine rig, such as: the overall efficiency, mass flow rate, and overall torque production, are provided and presented in this paper. The mass-averaged mean-flow quantities over the three-dimensional domain at blade-row outlet, obtained from AXOD2 simulations, such as: mean-flow Mach number, mean-flow angle, axial component of mean-flow Mach number, and the torque produced by the last rotor blade-row (the choked blade-row), are compared with results of the computational fluid dynamics (CFD) investigation presented in the Part-1 of the paper. The success and shortfall of the modeling-results of AXOD2, upon examination with experimental data published and with the CFD-investigation, are illustrated and addressed in this paper. As a simple modeling approach for supercritical flow, the performance of AXOD2 was found impressive.

1.0 Introduction

A two-dimensional, steady state, computational fluid dynamics (CFD) calculation over a two-dimensional, planar, axial-flow turbine rotor blade-row of a research aircraft engine was conducted and presented in Part-1 of the paper (Ref. 1). In it, quantitative data and trending of the time- and spatial-mean flow quantities, such as: mean-flow Mach numbers, mean-flow angle at rotor-discharge, tangential blade loading, mean-flow mass flux, and flow-path total pressure loss coefficients, were obtained and presented. Close resemblance to these behavior and trending were captured by the axial-flow turbine off-design computer code AXOD2 (Ref. 2), which is an extension to its predecessor-code AXOD (Ref. 3). The purpose of this paper is to provide and document the relevant mathematical formulas and the key modeling approach and model treatment, specifically for the supercritical flow treatment, currently implemented in AXOD2; and to illustrate the similarity and consistency of the result obtained from AXOD2 to the result and trending of the two-dimensional CFD-investigation presented in the Part-1 of the paper (Ref. 1). The head-to-head, quantitative comparison of the performance of AXOD2 to experimental data obtained in a three-dimensional, rotating turbine rig, published in References 4 and 5, are provided and presented in this paper. The success and shortfall of the results of AXOD2-simulation are illustrated and discussed.

AXOD/AXOD2 is highly analytical. Its construction follows mathematical principles and fundamental laws of gas dynamics rigorously. The analytical content and the mathematical derivations presented in this paper are originated from Reference 6.

Nomenclature

CFD	computational fluid dynamics
NACA	National Advisory Committee for Aeronautics
P&W	Pratt & Whitney Aircraft
2-D	two-dimensional
3-D	three-dimensional

Symbols

A	flow cross section area
cp	specific heat at constant pressure
G, J	unit conversion factor needed for the system of U.S. customary units
M	mean-flow Mach number
$\overline{M}$	three-dimensional mass-averaged mean-flow Mach number
M_x	axial component of mean-flow Mach number
$\overline{M_x}$	three-dimensional mass-averaged axial component of mean-flow Mach number
$\dot{m}$	mean-flow mass flux
P	static pressure
Pt	total pressure
R	specific gas constant
T	static temperature
Tt	total temperature
U	tangential blade velocity
V	mean-flow velocity
V_x	axial component of mean-flow velocity
w_r	total flow-mass-fraction including coolant flow mass-fraction
ρ	density
α	blade angle
β	mean-flow angle
$\bar{\beta}$	three-dimensional mass-averaged mean-flow angle
γ	specific heat ratio
η_B	blade-row efficiency
ω	mean-flow mass flow rate
ψ	mass flow parameter

Subscripts:

0	stator inlet
1	stator discharge

1A	rotor inlet
2	rotor discharge
0,1	interim state immediate after stator inlet
1A,2	interim state immediate after rotor inlet
critical	critical-flow quantity
i	radial-sector index
sector	sector's mean-flow quantity

Superscripts:

cool	coolant-flow property
ideal	ideal flow-property
isen	isentropic flow-property
$'$	quantity of the relative frame-of-reference

2.0 Mathematical Equations and Conditions

The complete description of the functionalities, capacities, and the mathematical bases of the computer code AXOD2/AXOD were presented in documentation-form in the previous publications of References 2 and 3. The loss-mechanisms, loss-modeling correlations, and the model-closure technique were introduced in Reference 7. The process and procedure conducted in the usage of code for problem solving, which invoked primarily the subcritical flow-treatment, were detailed in both References 7 and 8. Here the focus of discussion is on the supercritical flow-treatment currently implemented in AXOD2, which is a subject of matter entirely different from the subcritical flow-treatment of AXOD2.

The supercritical flow-treatment in AXOD2 is unique to the axial-flow turbine of aircraft engine. In that, the trailing edge of the turbine blade shape (or the flow passage) has no or has only a small to negligible amount of geometric divergence. In supercritical flow-condition, the sonic-line would spring out from the pressure-side corner of the blade-end into the flow passage confined by the blade-row geometry, and the flow at blade-row discharge would deflect by an angle against the blade trailing-edge angle, as such, the resulting discharge flow-angle would be smaller (in magnitude) than the blade-angle by a noticeable amount. The detailed flow picture of this is illustrated in Part-1 of the paper (Ref. 1) over a wide range of supercritical flow-conditions. The supercritical flow-treatment of AXOD2 captures these flow characteristics.

The mathematics and formulations applied to supercritical flow of AXOD2 are described hereafter. These equations are derived and presented thoroughly here, partly is because they are intriguing, and partly is for the purpose of documenting these for the record and for future reference. These mathematical relations and derivations are the bases of the code construction, and they have fundamental value.

In AXOD2, the supercritical flow-condition is identified as when

$$Pt^{ideal}/P > Pt^{ideal}/P_{critical} \tag{1}$$

In Equation (1), Pt^{ideal} is the ideal-total-pressure at the blade-row discharge station, P is the static pressure (actual) at blade-row discharge, and $P_{critical}$ is the static pressure of the critical-state, defined mathematically. $P_{critical}$ resides inside the blade-row passage when the flow at discharge is supercritical, the flow Mach number at the critical-state is one (1.0).

Pt^{ideal} is an idealized flow-quantity, where the flow is assumed isentropic in the flow-path, from a starting state at inlet to the blade-row discharge, defined in AXOD2 as

$$\left(Pt_1^{ideal} \big/ P_1 \right) = \left\{ \left[Pt_{0,1} \left(\frac{Tt_1{}^{isen}}{Tt_0} \right)^{\frac{\gamma}{\gamma-1}} \right] \Big/ P_1 \right\} \qquad (2)[1]$$

In Equation (2), the subscript 1 denotes the blade-row discharge station, subscript 0 denotes the blade-row inlet station, subscript '0,1' represents an interim state immediate after the blade-row inlet (see Ref. 2 for clarification on this.) The superscript 'isen' denotes the isentropic flow-property. An elaboration of this equation which relates the isentropic flow-properties to the actual flow-quantities is provided in Appendix A. This derivation is important because Tt^{isen} would have no meaning unless it is representable as a function of the actual physical and flow quantities.

The corresponding ideal-total-temperature Tt^{ideal} at the discharge station is defined (from the basic thermodynamic relation of gas) as

$$Tt_1^{ideal} \big/ T_1 = \left(Pt_1^{ideal} \big/ P_1 \right)^{\frac{\gamma-1}{\gamma}} \qquad (3)$$

Please note: Tt_1^{ideal} is not the same as Tt_1^{isen}. Tt_1^{ideal} is a thermodynamic quantity, exists through definition of Equation (3); whereas Tt_1^{isen} is an idealized flow-quantity, exists through an isentropic flow-process passing through a known point-of-state. They are fundamentally and thermodynamically different (see Appendix A for more detail).

Equation-forms 1, 2, and 3 are equally applicable to both the stator of the stationary (absolute) frame-of-reference, and the rotor of the rotational (relative) frame-of-reference. In fact, equations and derivations given in the main body of text of the paper are cast in forms that would equally be suitable for both the stator and the rotor. However, one should be mindful that the flow-quantities, e.g., total pressure, total temperature, flow velocity components, flow angles, and flow Mach numbers, are corresponding to their respective frames-of-reference, and they often do not possess the same number-value under different frames-of-reference; while the fluid-properties, such as static pressure, static temperature, fluid density, gas constants, molecular weight, etc. would be exactly the same in both frames-of-reference. The nomenclature adopted in the previous publications (e.g., Refs. 2, 7, and 8) puts a superscript 'prime' on the total pressure and total temperature as a reminder, indicating that they correspond to the flow-quantities of the relative frame-of-reference. Here in this paper, no separate nomenclature is used for different frames-of-reference, unless when there is possible ambiguity. For example, in Appendix A,

---

[1]Equation (2) presented here was given in Reference 2 as Equation (6S), however it was mistakenly expressed. The total temperatures Tt_1 should be the *isentropic* total temperature as that shown here, it should not be the *actual* total temperature expressed in Equation (6S) of Reference 2. Although under the modeling assumptions of AXOD2 the two would be the same when without the coolant-flow injection, but when there is an external heat-input, such as the coolant-flow addition, the actual total temperature at discharge, Tt_1, would be different from the isentropic total temperature, Tt_1^{isen}, at discharge. Furthermore, in the annulus region the flow should be stated as *frictionless*, instead of *isentropic* as that stated in Reference 2, since the treatment of AXOD2 does allow coolant-flow to be added in the annulus region. This, however, was merely an inappropriate classification, it does not change the fact that all modeling equations are applicable to the annulus region, with losses set to zero.

when represented by the actual physical quantities, Tt_1^{isen} takes on different forms with respect to the stator and the rotor due to the presence of external work-extract term of the rotor. In there, equations for the stator and equations for the rotor are written down in separate forms, otherwise it would be inappropriate and ambiguous. And that is the one situation, in this paper, where a single form-of-equation is not equally suited for both the stator and the rotor.

That said, to proceed with the supercritical flow-treatment, the code will first identify the critical-state. A key relation used for finding the critical-state is the blade-row loss formula applied in AXOD2, which links the *ideal* property-of-the-state at blade-row discharge to the *actual* property-of-the-state, is

$$[1 - Y_B] = \left(\frac{Tt_1 - T_1}{Tt_1}\right) \Big/ \left(\frac{Tt_1^{ideal} - T_1}{Tt_1^{ideal}}\right) \tag{4}$$

The Y_B is the blade-row kinetic energy loss-coefficient. It is regarded as a known (given) quantity, intrinsically provided by the loss-modeling and the loss-correlation of AXOD2 (the loss-mechanisms and the loss-model correlations were detailed in Refs. 2 and 7). Equation (4) here was given in Reference 2 as Equation (5S) of the stator, the corresponding equation applied to the rotor was Equation (5R) of Reference 2.

Let η_B denotes the blade-row efficiency which, by definition, equals $[1 - Y_B]$, we have

$$\eta_B = [1 - Y_B] = \left(\frac{Tt_1 - T_1}{Tt_1}\right) \Big/ \left(\frac{Tt_1^{ideal} - T_1}{Tt_1^{ideal}}\right) = \left(1 - \frac{T_1}{Tt_1}\right) \Big/ \left(1 - \frac{T_1}{Tt_1^{ideal}}\right) \tag{5}$$

Rearrange Equation (5), one can write

$$\left({}^{Tt_1}/_{T_1}\right) = 1 \Big/ \left(1 - \eta_B \left(1 - \frac{T_1}{Tt_1^{ideal}}\right)\right) \tag{6}$$

From the basic thermodynamic relation for gas, we can state

$$\left({}^{Pt_1}/_{P_1}\right) = \left({}^{Tt_1}/_{T_1}\right)^{\frac{\gamma}{\gamma-1}}$$

And thus, from Equation (6), we have

$$\left({}^{Pt_1}/_{P_1}\right) = \left[1 \Big/ \left(1 - \eta_B \left(1 - \frac{T_1}{Tt_1^{ideal}}\right)\right)\right]^{\frac{\gamma}{\gamma-1}} \tag{7}$$

Note that by setting η_B to one (1.0) in Equation (7), we get

$$\left(Pt_1^{ideal} \big/ P_1\right) = \left(Tt_1^{ideal} \big/ T_1\right)^{\frac{\gamma}{\gamma-1}}$$

which is the relation expressed previously by Equation (3). I.e., Pt_1^{ideal} is the actual physical Pt_1 excluding the presence and effect of blade-row loss Y_B.

Another relation involved in finding the critical-state is the flow Mach number. By definition

$$\frac{Tt_1}{T_1} = 1 + \left(\frac{\gamma-1}{2}\right) M_1{}^2$$

and thus

$$M_1 = \left[\left(\frac{2}{\gamma-1}\right)\left(\frac{Tt_1}{T_1} - 1\right)\right]^{\frac{1}{2}} \tag{8}$$

Now we are ready to define the critical state.

The critical state is defined as the critical-point along the path of a mass-flow-function. This mass-flow-function was derived in Shapiro (Reference 9, p. 82, eq. (4-11)) as

$$\left(\frac{\omega}{A}\right)\frac{\sqrt{Tt_1}}{P_1} = \sqrt{\frac{\gamma G}{R}}\, M_1 \sqrt{\frac{Tt_1}{T_1}} \tag{9}$$

Multiply a common factor of $\left(\frac{Pt_1^{ideal}}{P_1}\right)^{-1}$ to both side of Equation (9), we get

$$\left(\frac{\omega}{A}\right)\frac{\sqrt{Tt_1}}{Pt_1^{ideal}} = \sqrt{\frac{\gamma G}{R}}\, M_1 \sqrt{\frac{Tt_1}{T_1}} \left(\frac{Pt_1^{ideal}}{P_1}\right)^{-1} \tag{10}$$

Equation (10) was applied in Reference 6, but the equation itself was not revealed as it is presented here.

The reason $\left(\frac{Pt_1^{ideal}}{P_1}\right)^{-1}$ was used instead of $\left(\frac{Pt_1}{P_1}\right)^{-1}$ in Equation (10) is noted under Equation (7), that Pt_1^{ideal} does not explicitly contain the factor of blade-row efficiency η_B. Furthermore, the total temperature Tt_1 is the Tt_1^{isen} plus the coolant-flow temperature effect if there is coolant-flow addition to the blade-row passage (see Appendix A for this relationship). Tt_1^{isen} is free from the blade-row frictional loss. And the coolant-flow is regarded as a given heat-input, it too would have no direct dependency to the blade-row loss (or efficiency). The critical flow-mass-flux, $\left(\frac{\omega}{A}\right)_{critical}$, obtained from this equation (Eq. (10)) would then also be independent from the presence of blade-row loss, even when the flow in the blade-row passage is frictional and non-isentropic. Had the common factor $\left(\frac{Pt_1}{P_1}\right)^{-1}$being applied, the critical flow-mass-flux so obtained would be depending on the status of the blade-row loss. The critical flow-mass-flux, $\left(\frac{\omega}{A}\right)_{critical}$, will be defined and formulated later in detail.

Equation (10) is referred to as the mass flow function for the non-isentropic flow. The mass flow function for the isentropic flow was given in Reference 1 (Eq. (9)).

Put Equations (3), (6), and (8) into Equation (10), and let

$$\phi = \frac{Tt_1^{ideal}}{T_1} \tag{11}$$

Equation (10) can now be arranged into the form of

$$\left(\frac{\omega}{A}\right)\frac{\sqrt{Tt_1}}{Pt_1^{ideal}} = \sqrt{\frac{2\gamma G}{(\gamma-1)R}}\left(\eta_B\left(1-\frac{1}{\phi}\right)\right)^{\frac{1}{2}} \times \frac{1}{\left(1-\eta_B\left(1-\frac{1}{\phi}\right)\right)} \times \left(\frac{1}{\phi^{\frac{\gamma}{\gamma-1}}}\right) \tag{12}$$

Equation (12) is the form of equation revealed in Reference 6 (Flagg, p. 38).
Define a mass-flow-parameter, ψ. Let

$$\psi = \left.\left(\frac{\omega}{A}\right)\frac{\sqrt{Tt_1}}{Pt_1^{ideal}}\right/\sqrt{\frac{2\gamma G}{(\gamma-1)R}}$$

And let

$$X = \eta_B\left(1-\frac{1}{\phi}\right) \tag{13}$$

Equation (12) can now be written in the form of

$$\psi = X^{\frac{1}{2}}\,\frac{1}{(1-X)}\,\frac{1}{\left(\frac{\eta_B}{\eta_B-X}\right)^{\frac{\gamma}{\gamma-1}}} \tag{14}$$

where in Equation (14), deducible from Equation (13),

$$\frac{\eta_B}{\eta_B-X} = \phi \tag{15}$$

The mass flow parameter, ψ, has a critical-point (the maximum) along its path-of-curve with respect to ϕ. The critical-state is referring to the properties-of-state at this critical point. I.e., at the point where

$$\frac{d\psi}{d\phi} = 0$$

with (γ, G, R, η_B) considered as given constants.
Write

$$\frac{d\psi}{d\phi} = \frac{d\psi}{dX}\,\frac{dX}{d\phi} = 0$$

The critical-point can reside at $\frac{d\psi}{dX} = 0$, or, at $\frac{dX}{d\phi} = 0$.
However, from Equation (13),

$$\frac{dX}{d\phi} = \eta_B\,\frac{1}{\phi^2}$$

If $\frac{dX}{d\phi} = 0$, then $\phi \longrightarrow \infty$, which leads to a physically unrealizable solution. Thus, one concludes, the critical-point resides at the condition when

$$\frac{d\psi}{dX} = 0 \tag{16}$$

This critical-point condition, Equation (16), was also noted in Reference 6.

By differentiating Equation (14) with respect to *X*, Equation (16) was solved. The outcome is given here, the step-by-step arithmetic for this is provided in Appendix B.

The solution of Equation (16) lies at

$$X_{critical} = \left(-B - \sqrt{B^2 - 4AC}\right) \Big/ (2A) \tag{17}$$

where

$$A = \left(\frac{\gamma}{\gamma - 1}\right) - \frac{1}{2}$$
$$B = -\left[\left(\frac{\gamma}{\gamma - 1}\right) + \frac{1 - \eta_B}{2}\right]$$
$$C = \frac{\eta_B}{2}$$

Equation (17) and the A, B, C, are presented here in the same forms as those that were given in Reference 6. But again, no detail was given in Reference 6 as to how this result was obtained.

From Equations (11) and (15), we now have

$$\phi_{critical} = \left(\frac{Tt_1^{ideal}}{T_1}\right)_{critical} = \frac{\eta_B}{\eta_B - X_{critical}} \tag{18}$$

Let the critical state be along the path of varying static temperature *T*, with its referencing state be at the blade-row discharge station. We can define, formally, that

$$\phi_{critical} = \left(\frac{Tt_1^{ideal}}{T_{critical}}\right) = \frac{\eta_B}{\eta_B - X_{critical}} \tag{19}$$

And thus, from Equation (19),

$$T_{critical} = Tt_1^{ideal} \Big/ \left(\frac{\eta_B}{\eta_B - X_{critical}}\right) \tag{20}$$

where, $X_{critical}$ was defined and is obtainable through Equation (17).

The $P_{critical}$ is defined through the isentropic relation of

$$\left(Pt_1^{ideal} \Big/ P_{critical}\right) = \left(Tt_1^{ideal} \Big/ T_{critical}\right)^{\frac{\gamma}{\gamma - 1}} \tag{21}$$

Rearrange Equation (21), we have,

$$P_{critical} = {Pt_1^{ideal}} \Big/ \left({Tt_1^{ideal}} \big/ {T_{critical}} \right)^{\frac{\gamma}{\gamma-1}}$$

$$= {Pt_1^{ideal}} \Big/ \left(\frac{\eta_B}{\eta_B - X_{critical}} \right)^{\frac{\gamma}{\gamma-1}} \tag{22}$$

From Equations (17), (20), and (22), we now know the critical static temperature, $T_{critical}$, and the critical static pressure, $P_{critical}$, referencing to the ideal total temperature and the ideal total pressure at the blade-row discharge station, the Tt_1^{ideal} and the Pt_1^{ideal}.

Pt_1^{ideal} is found from Equation (2), Tt_1^{ideal} is found from Equation (3), when the static pressure and temperature at the discharge station, P_1 and T_1, are determined through the process of solving the system equations. $T_{critical}$ and $P_{critical}$ are thus fully quantified and obtainable.

3.0 Critical Flow-Mass-Flux and Supercritical Flow-Treatment of AXOD2

The principle of supercritical flow-treatment in AXOD2 lies under the assumption that the blade-row discharge mass-flow-rate remains to be a constant in all supercritical flow conditions. This principle invokes two postulations: (1) the choked-flow mass-flow-rate remains the same as the critical mass-flow-rate of the blade-row passage, and (2) the effective flow area normal to the critical flow-velocity remains the same in all supercritical flow-conditions. Of course, these are idealized propositions, in reality neither of the two may be held exactly true in supercritical flow conditions, however they are the modeling assumptions applied (with provisional measures) in AXOD2, and they are realistically accurate.

We shall first define the critical flow-mass-flux through the following derivations.

The equation of state applied in AXOD2 is the perfect gas law of

$$P = \rho RT$$

From Equations (20), (22) and the equation-of-state, one has

$$\rho_{critical} = {P_{critical}} \big/ {(R\ T_{critical})} \tag{23}$$

The critical flow-velocity (referring to the total velocity here) is when flow Mach number (absolute-value for the stator and relative-value for the rotor) is one (1.0), i.e., the critical flow-velocity is the local sonic velocity. Thus,

$$V_{critical} = \sqrt{\gamma G R T_{critical}} \tag{24}$$

The flow-mass-flux is the density times the flow velocity, thus the critical flow-mass-flux is

$$\dot{m}_{critical} = \rho_{critical}\, V_{critical} = P_{critical} \sqrt{{\left(\frac{\gamma G}{R}\right)} \Big/ {T_{critical}}} \tag{25}$$

In AXOD2, Equations (23) to (25) are sought, after $T_{critical}$ and $P_{critical}$ were solved for and were obtained from Equations (20) and (22).

Noted here: a very important characteristics of the critical flow-mass-flux formulated in AXOD2, is that its value stays unchanged even when the $\left(\frac{Pt_1^{ideal}}{P_1}\right)$ and the actual $\left(\frac{Tt_1}{T_1}\right)$ in Equation (10) at the discharge station are changing under different supercritical flow conditions, because it is the value of the critical-point along the path defined by the mass-flow-function (Eq. (10)) that is sought and obtained. Although the mass-flow-parameter (ψ) of the mass-flow-function varies from point to point on that path (from one supercritical flow-condition at discharge to another), but the critical-point is a unique (fixed) point on the curve, and its value does not change with respect to the end-state specified at discharge. Another important characteristic, as noted previously, is that the critical flow-mass-flux so obtained (Eq. (25)) is independent to the blade-row efficiency η_B (or equivalently, the blade-row frictional loss Y_B), the reason for this was stated and explained in Section 2.0, under Equation (10) for the non-isentropic mass-flow-function. These characteristics will be demonstrated later by Figure 1.

The critical mass-flow-rate, $\omega_{critical}$, is the multiplication of $\dot{m}_{critical}$ to A_{norm}, where A_{norm} is the effective cross-section-area normal to the critical flow velocity.

$$\omega_{critical} = \dot{m}_{critical}\, A_{norm} \tag{26}$$

In AXOD2, A_{norm} is approximated by

$$A_{norm} = A_1 \times (1 - Y_c) \times cos(\alpha_1) \tag{27}$$

where, A_1 is the geometric sector-area of the annulus at the blade-row discharge station, the $(1 - Y_C)$ is the flow area blockage-factor due to viscous boundary-layer effect at discharge, and α_1 is the tangential blade angle (tangent to the axial-plane, not to the meridional-plane) at the blade-row discharge. Provision was made in AXOD2 that A_{norm} does not vary in supercritical flow-conditions, specifically, $(1 - Y_c)$ stands un-corrected in the supercritical flow-regime.

The mass-flow-rate of the sector at blade-row discharge is defined and calculated in AXOD2 as

$$\omega_{sector} = \rho_1 \times V_{x_1} \times A_1 \times (1 - Y_c) \qquad (28)^2$$

where ρ_1 is the fluid density at sector discharge, V_{x_1} is the axial component of the mean-flow velocity at sector-discharge, $A_1 \times (1 - Y_c)$ is the effective sector-flow-area at blade-row discharge, normal to the axial mean-flow-velocity. Equation (28) is applied consistently in AXOD2 to every sector at every blade-row discharge, as this is the way mass-flow-rate is calculated and recorded in AXOD2 (the total mass-flow-rate at a blade-row discharge station is the sum of the individual mass-flow-rate of the sectors).

The Y_c is the flow area blockage-loss-factor applied to the equation of mass-conservation in AXOD2. The model-correlation of Y_c and its implication to the overall flow-momentum loss were described and discussed in References 2 and 7.

3.1 Supercritical Flow-Treatment of AXOD2

When the pressure ratio ${Pt_1^{ideal}}/{P_1}$ at the blade-row discharge exceeds ${Pt_1^{ideal}}/{P_{critical}}$, the mass-flow-rate, ω_{sector} of Equation (28), is instantly assigned to the value of the critical mass flow rate, obtained from Equations (26) and (27). And the flow solution is sought under a chain of incrementally increasing pressure ratios across the choked blade-row. This treatment is applied onto every radial-sector

[2]The mass flow rate at sector-discharge expressed by Equation (28) includes coolant-flow-mass contribution to the sector, should there be coolant-flow injected into the blade-row passage. The net mass-flow-rate at sector discharge (Eq. (28)) cannot exceed a critical value (the critical mass-flow-rate), which is represented here by Equations (26) and (27).

of the blade-row passage individually. This is very different from the treatment applied to the subcritical (continuous) flows, in that, the mass-flow-rate and the pressure-ratio across the blade-row are co-dependent in subcritical-flow, meaning that, if the flow rate is given (assigned) then the pressure ratio is determined in correspondence; contrarily, if the pressure ratio across the blade-row is known (assigned) then the flow rate is determined in correspondence. In supercritical flow-treatment, however, both the mass-flow-rate and the pressure-ratio across the blade-row are assigned (given) concurrently. This poses a fundamental problem to the solution-solving logic, that the constraints are potentially over-specified with respect to the available degrees-of-freedom in the mathematical solution. But luckily, an extra degree-of-freedom can be added to the supercritical flow-treatment, which is the tangential-flow-angle at the blade-row discharge. In subcritical-flow the tangential flow angle at the blade-row discharge is assigned to the representative-blade-angle at discharge, which is a required input to the code (a pre-determined quantity given through the namelist-input). That means the tangential-flow-angle at discharge is an invariant (a fixed value) in the subcritical flow-treatment. In supercritical-flow, in order to gain the extra degree-of-freedom, one has to allow this discharge tangential-flow-angle to be varied with respect to the supercritical pressure-ratio imposed. That means it can no longer stay the same as the given discharge blade-angle in supercritical out-flow conditions.

In AXOD2, in supercritical flow-conditions, the tangential-flow-angle is calculated in the manner that the mass-flow-rate at the blade-row discharge would match the critical mass-flow-rate defined and calculated from Equations (26) and (27). It turns out that the discharge tangential-flow-angle has to deflect against the direction of the blade-angle, such that the effective discharge flow angle becomes smaller (by magnitude), which would reduce the fraction of the tangential-flow-velocity and would increase the fraction of the axial-flow-velocity, with respect to the total-velocity at the blade-row discharge, which in term would increase the resulting mass-flow-rate passing through the effective flow area available at the plane of blade-row outlet, and be able to maintain the mass-flow-rate a constant (equals to the critical mass-flow-rate obtained), at all imposed supercritical flow pressure-ratios. If the tangential flow angle at discharge is not deflected (i.e., driven away from the flow-path defined by the blade-passage), the mass-flow-rate at the blade-row discharge would naturally decrease in the supercritical flow regime, as that discussed in Part-1 of the paper (Ref. 1) and cited in the literature (e.g., Shapiro, Ref. 9, p. 76, Fig. 4.3).

3.2 Demonstration of Supercritical Flow-Treatment in AXOD2

The supercritical flow-treatment of AXOD2 is demonstrated here by Figure 1. This case was experimentally studied in Reference 5. It is a (3 and 1/2)-stage axial-flow turbine with high blade-loadings. Comprehensive comparison between AXOD2 simulation-result and the experimental data published in Reference 5 are given later in Section 4.0. Here only the sector-behavior of the mass-flow-rate and the flow-angle at the last rotor discharge, obtained from AXOD2 simulation, are shown. Three sectors: hub, pitch (mean), and tip, out of the total of five radial-sectors are plotted. They are shown here to demonstrate the supercritical flow-treatment of AXOD2, described in the preceding section.

In Figure 1, the abscissa is the inlet-total (relative) to discharge-static (actual) pressure ratio across the rotor. The total and the static pressures were radially, mass-averaged quantities. The square-symbol on the plot denotes the first occurrence where all radial-sectors of the blade-row passage were found choked. I.e., the condition that

$$Pt_1^{ideal}/P_1 > Pt_1^{ideal}/P_{critical}$$

existed at the rotor discharge on every sector. Beyond this point, the flow at discharge is in the supercritical flow-condition (regime).

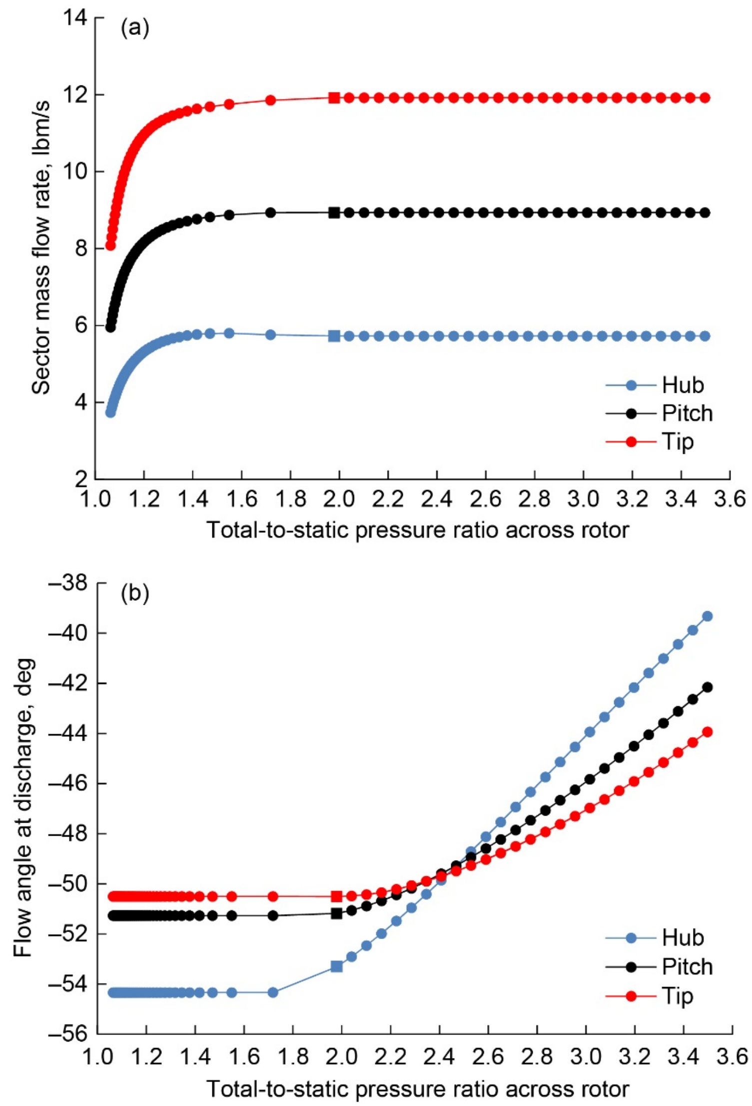

Figure 1.—Sector behavior at last rotor discharge at 100 percent speed. (a) Mass flow rate. (b) Flow angle.

In Figure 1(a), the sector mass-flow-rate remains to be constant at all supercritical pressure ratios (supercritical flow-conditions). Each sector possessed a different flow rate (and correspondingly, a different critical flow-mass-flux), which is the critical mass-flow-rate calculated, and re-calculated, individually at each sector of the blade-row passage, at every incrementally increasing supercritical pressure-ratio imposed. The critical mass-flow-rate obtained does not change under the different supercritical flow-conditions, even with the changing blade-row efficiency η_B due to loss-corrections applied to supercritical-flow regime, as those mentioned in Part-1 of the paper (Ref. 1), which will be provided in detail later in Section 3.4. In Figure 1(b), the square-symbols of the first choke-point indicate that, although all sectors are choked, however the tip-sector is barely choked while the hub-sector is already beyond-choked. The flow angle at the hub-sector discharge has deflected by about 1°, while at tip-sector the discharge-flow-angle is barely deflected. As the pressure-ratio increases, the flow-angle at discharge deflects more. The amount of flow-angle deflection at a supercritical flow pressure-ratio can be substantial, up to 15° at the hub-sector as shown in Figure 1(b). The reason is that, as stated in Section 3.1, the flow-angle at discharge is co-dependent to the mass-flow-rate in the supercritical flow-treatment of AXOD2, that flow-angle deflects, such that the resulting mass-flow-rate at the sector-discharge can remain as constant. The plots shown here demonstrated the supercritical flow-treatment implemented in AXOD2, as described and discussed in the previous sections (Sections 3.0 and 3.1). Again, the theoretical behavior of a one-dimensional flow is that the mass-flow-rate would decrease in supercritical flow-regime, had the flow not deflected at discharge.

3.3 Limit-Loading Condition for Three-Dimensional Axial-Flow Turbine

Following the argument made in Part-1 of the paper, the quantitative definition of the limit-loading condition is that when the normal component of the mean-flow Mach number at discharge reached the value of one (1.0) in a turbine blade-row where the blade shape has no or has only a small to negligible amount of geometric divergence at discharge (Ref. 1). The direction-normal is normal to the effective flow area at the blade-row outlet plane. For a two-dimensional axial-flow turbine, this direction-normal is the axial direction at the blade-row discharge, and the appropriate normal-component of flow Mach number is the axial component of the mean-flow Mach number, M_x, which is obvious (for the 2-D turbine blade-row) and was explained and demonstrated in Reference 1. For a three-dimensional turbine blade-row, the appropriate effective flow area, and the direction-normal at the blade-row outlet are not so obvious. In AXOD2, at the blade-row discharge, the effective flow area is taken to be the summation of the effective-flow-area of the sectors, where the effective-sector-flow-area is taken as the sector annulus area subtracting the displacement thickness of the boundary-layer at the discharge station, as that shown by Equation (28). The direction-normal of this effective sector-flow-area is the axial-direction. The normal component of the mean-flow Mach number for the three-dimensional turbine blade-row at geometric outlet applied in AXOD2, is the mass-averaged discharge axial-flow Mach number obtained at each sector, as

$$\overline{M_x} = \sum_i \left(\omega_i \times M_{x_i}\right) \Big/ \sum_i \omega_i \tag{29}$$

In Equation (29), the ω_i is the mass-flow-rate at the sector discharge, M_{x_i} is the axial-component of mean-flow (mean over the sector effective-flow-area) Mach number at sector discharge. $\overline{M_x}$ represents the axial-component of the mean-flow (mean over the 3-D figure) Mach number of the three-dimensional turbine blade-row at the discharge station. This definition (representation) is consistent with how the turbine mass-flow-rate is calculated at the blade-row discharge station in AXOD2.

Equation (29) is a discrete representation of the actual three-dimensional turbine flow at discharge. This definition is appropriate even when the turbine blade-row is tapered, because tapering physically does not alter (increase or decrease) the effective flow area, nor the direction-normal, at the geometric outlet, since tapering does not impose a geometric constraint for additional radial flow-component to be created. It is also appropriate when the blade-row geometry has end-wall contouring. The effective outlet-flow-area at sector-discharge is still the effective sector-annulus-area, and the direction-normal to this effective flow-area is the axial-direction; however, when there is end-wall contouring, the effective geometric area-expansion-ratio, with respect to the direction-normal, of the three-dimensional blade-row passage would need to include the contribution from the end-wall contouring, which in term could change the extremum (the theoretical limiting-value) of the axial-component of mean-flow Mach number, $\overline{M_x}$, at the blade-row discharge station.

Equation (29) is the working definition of the *formal* limit-loading condition for three-dimensional axial-flow turbine. When there is no appreciable geometric divergence, the limiting value (extremum) of $\overline{M_x}$ at the last rotor discharge would be one (1.0). Therefore, the quantitative definition of the *formal* limit-loading condition for the three-dimensional, axial-flow turbine of the aircraft engine can be stated (proposed) as: when the last rotor-discharge of the turbine assembly reached the condition of

$$\overline{M_x} = \sum_i \left(\omega_i \times M_{x_i}\right) \Big/ \sum_i \omega_i = 1 \tag{30}$$

As that discussed, illustrated and observed in Part-1 of the paper (Ref. 1) from the two-dimensional CFD investigation, of which its conclusion is extended here to the general three-dimensional axial-flow turbines, is that: when $\overline{M_x}$ reached its extremum (1.0 for a constant area expansion channel) in supercritical-flow at the last rotor (the choked blade-row) discharge, the expansion process in the axial-flow turbine would cease, and physically the time-mean flow properties at, and at upstream of, the discharge station of the over-expanded rotor would stay unchanged thereafter. In supercritical-flow calculation in AXOD2, program execution is set to terminate (cut-off) at this limit-loading condition (of Eq. (30)), since AXOD2 is an analytical model-representation of the three-dimensional, axial-flow turbine with little or no geometric divergence at the blade-row discharge. No further march-on calculation with higher pressure-ratio is made in AXOD2 at 'beyond' this limit-loading condition. Although physically and computationally the flow solutions do continue to exist under the constant trending as that shown in Ref. 1, however analytically the AXOD2-model breaks down soon after the condition of $\overline{M_x} = 1$ is reached. An alternative to this *formal* definition of the limit-loading condition is introduced in the Results and Discussion section (Section 4.0) of the paper and will be discussed at length there.

3.4 Blade-Row Efficiency Correction Function in Supercritical Flow Conditions

The blade-row efficiency, η_B, in AXOD/AXOD2 was corrected for the shock-loss in the flow-path in supercritical flow-conditions. The justification for this was described graphically by Figure 11 of Reference 1 (Part-1 of the paper).

In AXOD (Ref. 3), this corrected η_B was defined as

$$(\eta_B)_{corrected} = \eta_B \times \eta_{mod} \tag{31}$$

The η_B in Equation (31) is the intrinsically determined blade-row efficiency from the built-in loss correlation.

And

$$\eta_{mod} = a\left(\frac{Pt_1^{ideal}}{P_1}\right)^3 + b\left(\frac{Pt_1^{ideal}}{P_1}\right)^2 + c\left(\frac{Pt_1^{ideal}}{P_1}\right) + d \tag{32}$$

with

$$a = 0.011852$$
$$b = -0.115556$$
$$c = 0.355555$$
$$d = 0.64815$$

and with the conditions that

$$\eta_{mod} = 1.0 \text{ when } \left(\frac{Pt_1^{ideal}}{P_1}\right) = 2.5$$
$$\eta_{mod} = 0.98 \text{ when } \left(\frac{Pt_1^{ideal}}{P_1}\right) = 4.0$$

When the pressure ratio is less than $\left(\frac{Pt_1^{ideal}}{P_1}\right) = 2.5$, $\eta_{mod} = 1.0$ stands; and when the pressure ratio is greater than $\left(\frac{Pt_1^{ideal}}{P_1}\right) = 4.0$, $\eta_{mod} = 0.98$ remains.

Currently in AXOD2, Equation (32) has been changed to a simpler linear function of

$$\eta_{mod} = 1.0 + (\eta_{low} - 1.0) \times \frac{\left| PR_1 - \left(\frac{Pt_1^{ideal}}{P_1} \right) \right|}{|PR_1 - PR_2|} \tag{33}$$

where,

$$\eta_{low} = 0.97$$
$$PR_1 = 2.0$$
$$PR_2 = 5.0$$

When the pressure ratio is less than $\left(\frac{Pt_1^{ideal}}{P_1}\right) = 2.0$, $\eta_{mod} = 1.0$ stands; and when the pressure ratio is greater than $\left(\frac{Pt_1^{ideal}}{P_1}\right) = 5.0$, $\eta_{mod} = \eta_{low} = 0.97$ remains.

The set-constants of Equation (33) are easier to be modified. The results and the trending obtained with Equation (33) were as good as, if not better than, that of Equation (32).

4.0 Results and Discussion

Two cases were selected for the purpose of capability demonstration and performance evaluation of the computer code AXOD2, in head-to-head comparisons with experimental data published.

The first case was a (4 and 1/2)-stage lift-fan turbine with very high stage-loading factors (4.66 on average), as described in Reference 4. The second case was a (3 and 1/2)-stage fan-drive turbine, also with high loadings (4.0 on average), described in Reference 5.

The two cases are particularly of interest to the present study, because they were highly loaded turbines that were designed to operate at beyond-choked conditions (supercritical outflow at the last rotor discharge). As such, the experimental works of References 4 and 5 had extended well into the supercritical flow-regime, with data available up to the point of the limit-loading condition. Data published in References 4 and 5 include: turbine mass-flow-rate, overall turbine total efficiency, and the most among all valuable data, the overall turbine torque production. These data are perfectly suited for the purpose of validating and evaluating the supercritical flow-treatment of AXOD2.

Experimental data were converted and presented in forms of equivalent flow-quantities, with reference to the equivalent flow-conditions (the NACA standard air conditions, in these works) at turbine inlet. The turbine inlet flow-conditions and the turbine speed-of-rotation applied in AXOD2-simulations were these equivalent flow-conditions and the equivalent speed-of-rotation reported by the experiments. Detailed information regards to the equivalent flow-conditions and the equivalent flow-quantities can be found in Reference 10 (p. 58).

The two cases have been studied before using AXOD2 and results from that study were presented in Reference 8. The present work builds on the foundation established in that study, utilizes the optimum loss-coefficients found and re-worked the two cases to cover more speed-lines of 70, 80, 90, and 100 percent speed. The experimental data of References 4 and 5 had also included 110 and 120 percent speed, however, in the study of Reference 8 it was found that unexplainable discrepancies existed between AXOD2 results and the experimental data at over-speed, specifically at the 120 percent speed-line, in both case-studies. Since the experiments were done decades ago and there is no possibility to re-do the experiment now, it was decided not to compare the AXOD2-results with experimental data of the 110 percent speed and the 120 percent speed presented in References 4 and 5.

The two case-comparisons are presented in separate hereafter.

4.1 NASA/P&W Four and One-Half (4 ½)-Stage Lift-Fan Turbine

The process and procedure of the AXOD2 simulation are exactly the same as that described in Reference 8. The same optimum loss-coefficients obtained in Reference 8 were applied to this work. Five radial-sectors were given to cover the flow passage. The result-comparisons of the overall total efficiency, equivalent mass-flow-rate, and the overall equivalent-torque produced are presented in Figures 2 to 4, respectively. The abscissa is the overall total (absolute) -to- total (absolute) pressure ratio across the turbine assembly. Experimental data were published in Reference 4.

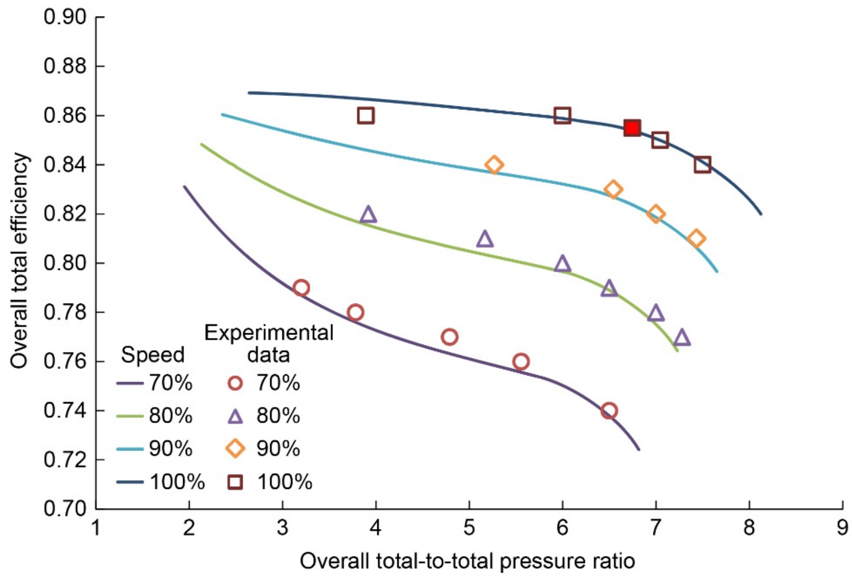

Figure 2.—NASA/P&W (4½)-stage lift-fan turbine. Comparison of overall total efficiency between AXOD2 simulation-result and experimental data of Reference 4.

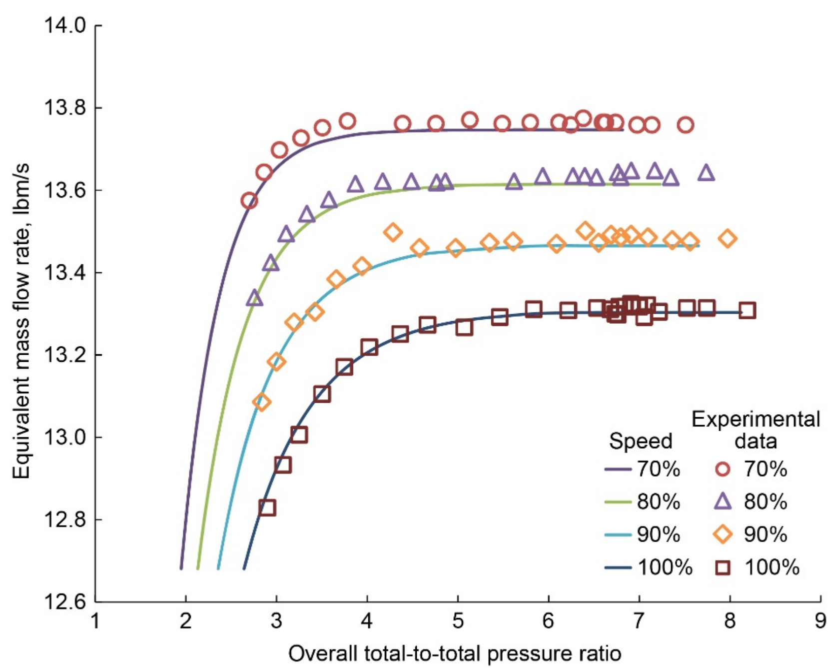

Figure 3.—NASA/P&W (4½)-stage lift-fan turbine. Comparison of equivalent mass flow rate between AXOD2 simulation-result and experimental data of Reference 4.

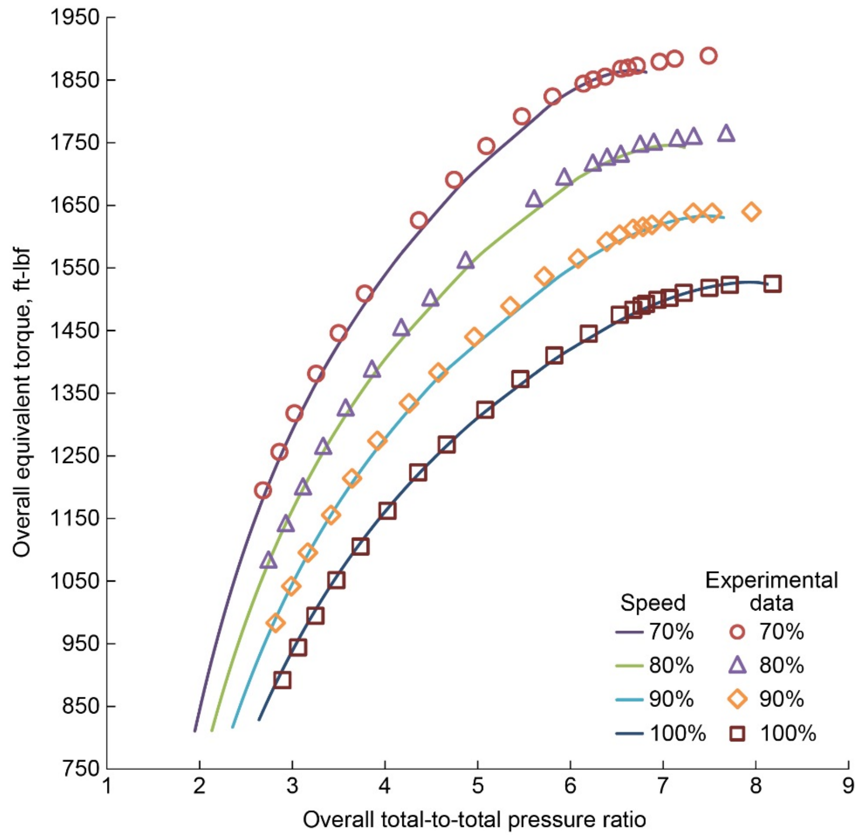

Figure 4.—NASA/P&W (4½)-stage lift-fan turbine. Comparison of overall equivalent-torque between AXOD2 simulation-result and experimental data of Reference 4.

The solid red-block at 100 percent speed-line in Figure 2 is the design-point identified by the experiment. The experimental data presented here were scanned and digitized from plots of Reference 4. The AXOD2 simulations covered a wide range of flow conditions, from subcritical- to supercritical- flow. Program execution was terminated at the formal limit-loading condition, as specified by Equation (30).

The match between the AXOD2-results and the experimental data were impressive. Of particular interest was the torque-comparison. The AXOD2 calculations of torque were quite good when compared with the experimental torque-measurements, over the range of pressure-ratios up to the point near the limit-loading condition. The trending and performance of the torque-production exhibited by AXOD2 is noteworthy and is rarely seen from other analytical methods-of-prediction or computer codes of the same level-of-fidelity as AXOD2.

The success of AXOD2-predicition on torque is rooted at the supercritical flow-treatment of AXOD2. The key requirement of this treatment, as noted at the beginning of Section 3.0, is that the mass-flow-rate remained constant in all supercritical flow-conditions. In order to satisfy this modeling requirement, the flow at the choked-rotor (the last rotor) discharge would have to deflect against the blade-angle at discharge to reduce the tangential-velocity and increase the axial-velocity, proportionally with respect to the total-velocity. This change in the discharge flow-velocities affects not only the mass-flow-rate passing through the blade-row passage, but also, simultaneously, altered the specific torque-production over the rotor blade-row. The change in specific-torque is due to the change brought to the tangential flow-velocity at blade-row discharge. This can be understood by examining the balance-equation of the angular momentum conservation, e.g., Equation (7R) given in Reference 2. The combination of the flow-rate increase (actually, maintained as constant, as opposed to natural-decrease had the discharge-flow not been specially treated, as noted in Section 3.1) and the tangential flow-velocity decrease (due to flow-angle deflection) has changed the torque-profile of the last rotor at beyond-choke. The end result of this change is the close match of the torque-predication by AXOD2, comparing to the measured-torque by experiment at different speed-lines.

Upon closer examination of Figure 4, a couple shortcomings became clear. The first was that the pressure ratio at the predicted limit-loading condition, Equation (30), is short, somewhat lower than the pressure ratio indicated by the experimental data. This is more evident at the lower speed-line (70 percent speed) than at the higher speed-line (at 100 percent speed). The second noticeable shortfall, was that the torque predicted by AXOD2 is not monotonically increasing, but passed a peak (maximum) value, and dropped down in the region near the end of the point of limit-loading condition (again, referring to the point where Equation (30) was met.) This drop-down of torque has occurred on every speed-line investigated.

The reason for the two shortfalls, is because the supercritical flow-treatment of AXOD2 is simply a one-dimensional modeling-treatment of the effect of the actual, physical occurrence of the characteristic waves (shock waves and expansion waves) at the choked blade-row discharge. The physical appearances of the characteristic waves were graphically illustrated clearly and comprehensively in Part-1 of the paper (Ref. 1). The presence of these shock-waves and expansion-waves is highly two-dimensional (nonuniform) in nature, while the modeling-treatment of AXOD2 on the supercritical-flow is a one-dimensional model-treatment that simply enforces a uniform streamline-deflection at the sector discharge, to maintain the flow-rate as a constant in the supercritical flow-conditions. Which, in effect is only mimicking the discharge flow-deflection owing to the presence of the physical characteristic waves. Apparently, this modeling approach is quite adequate (even accurate) and successful at the lower portion of the supercritical flow-regime, but as the limit-loading condition draws near, the two-dimensionality of the characteristic wave-intensity and the wave-distribution becomes more dominant, that the structure of the flow at blade-row discharge becomes highly two-dimensional and distributed unevenly across the blade-row outlet, with much higher intensity near the blade-row trailing edge than that across the larger portion of the flow passage at discharge. This intensified, highly uneven distribution apparently evoked a different physical flow momentum and energy transfer-mechanism at close to the blades, that in effect holds-up and extends the development of the limit-loading condition, such that the actual location of the pressure-ratio where the limit-load matured is further down than that predicted by the uniform-approximation of the AXOD2 modeling-approach. The peak-value (and the drop-down thereafter) of the blade-loading (or torque) should not have physically existed. Rather, the blade-loading should be saturating into a constant trend monotonically, as that illustrated by Figure 5 of Reference 1 (the Part-1 of the paper).

The impact of this highly uneven, two-dimensional distribution of the characteristic waves across the outlet plane is that the one-dimensional supercritical flow modeling-treatment of AXOD2 breaks down in the region near the point of the limit-loading condition. In fact, if the simulation passed beyond the point of limit-loading condition, i.e., at a pressure-ratio higher than that of the condition of $\overline{M_x} = 1$ (Eq. (30)), negative static pressure or temperature results soon after, and the program execution would fail. This suggests that the one-dimensional supercritical flow-treatment of AXOD2 is physically adequate and accurate, up to and only up to the point of the peak-of-torque (illustrated in Fig. 4). Beyond the occurrence of the peak-torque, the two-dimensional nature of the supercritical flow structure became dominant, and the AXOD2-simulation became invalid.

Because of this, an alternative definition of the limit-loading condition that suits AXOD2 supercritical flow modeling-treatment is suggested as being the supercritical pressure-ratio where

$$Torque = maximum \qquad (34)[3]$$

[3]Torque (of rotor) in AXOD2 is calculated as the power-output divided by the rotor angular speed-of-rotation. The power-output of a rotor sector is the sector specific work-extract (see Ref. 2 for its definition) times the rotor inlet sector-mass-flow-rate. The torque of a rotor blade-row would then be the summation of the sector-mass-flow-rate at rotor-inlet times the specific-work-extract of the rotor sector, then divided by the angular speed-of-rotation of the rotor. The overall-torque of the turbine is the sum of all torques produced by the rotors of the turbine assembly.

Equation (34) is referred to as the physical limit-loading condition of AXOD2, while Equation (30) is the mathematical, *formal* limit-loading condition of the axial-flow turbine. The supercritical flow-solution of AXOD2 is in fact ill-behaved and physically inadequate in region beyond the occurrence of this peak-of-torque. Therefore, in AXOD2-simulation, one may wish to accept the limit-loading condition to be as Equation (34), instead of as Equation (30) which would contain a portion of ill-behaved solution. This is the limitation of the supercritical flow-treatment of AXOD2, that the model breaks down after the point of peak-of-torque.

It, however, is quite interesting and is noted in particular here, that for all cases tested or studied with AXOD2, this peak-of-torque has always existed, and has always occurred before the *formal* limit-loading condition is reached. Were it not for the work of Reference 1, where the tangential blade-loading was clearly shown merged (saturated) smoothly into the constant value with no downward trend, one might think this peak-of-torque of AXOD2-result is physical, not as an anomaly. But make no mistake about this, it is an anomaly. The downward trending shown by AXOD2-result is not physical, as the AXOD2-simulation would fail soon after the condition of Equation (30) were met, and this is known to be untrue. CFD-investigation conducted in Reference 1 has indicated flow structures (flow solutions) do continue to exist under much higher pressure-ratios imposed, than the pressure-ratio observed at the limit-loading condition.

Some more plots, namely the mean-flow Mach numbers, mean-flow angles, and the axial-component of mean-flow Mach number, at the last-rotor discharge station (post-processing solution over the rotor-4 alone), obtained from AXOD2-simulation, are given in Figure 5. They illustrate the similarity and the contrast between the CFD-results shown by Figure 3 of Reference 1 (the Part-1 of the paper) and the AXOD2-results of the one-dimensional modeling approach. The trending between the two are similar, which again, is an indication that the model-treatment of AXOD2 is analytically justifiable. However, the variations (patterns) shown by AXOD2-result are more uniform (linear) than that shown by Figure 3 of Reference 1. The reason for this, partly is because shown here are the behavior of the flow-quantities averaged across the three-dimensional outlet plane at the blade-row discharge station, while those in Figure 3 of Reference 1 were the results reduced (averaged) from a two-dimensional, planar, blade-row calculation, which has not being smeared-out across the variation of a three-dimensional domain; and partly is because AXOD2-modeling is one-dimensional, while shown in Figure 3 of Reference 1 is the outcome of a two-dimensional CFD-simulation, the effect of the two-dimensionality (the curvature) at the tail-end portion of the profile (of Fig. 3 in Ref. 1) was not captured in AXOD2-modeling.

The abscissa in Figure 5 is the mass-averaged inlet-total-pressure (relative) to mass-averaged discharge-static-pressure (actual) across the last rotor (rotor 4) of Reference 4. The ordinates are the mass-averaged flow quantities over the three-dimensional plane-of-exit at the rotor-discharge, as:

$$\bar{M} = \sum_i(\omega_i \times M_i) \Big/ \sum_i \omega_i \tag{35}$$

$$\bar{\beta} = \sum_i(\omega_i \times \beta_i) \Big/ \sum_i \omega_i \tag{36}$$

$$\overline{M_x} = \sum_i\left(\omega_i \times M_{x_i}\right) \Big/ \sum_i \omega_i \tag{37}$$

At above, ω_i is the sector's mass-flow-rate, M_i, β_i, M_{x_i} are the sector's effective-flow-area averaged flow Mach number, flow angle, and the axial-component of flow Mach number, respectively at each sector discharge. Plotted here are the results of a rotor blade-row, therefore the Mach numbers and the flow angles should be understood as referring to flow-quantities of the relative (rotational) frame-of-reference.

A noteworthy point about Figure 5, is that the plots of mass-averaged, mean-flow properties at the three-dimensional blade-row discharge appear to be independent to the speed-of-rotation. I.e., all curves in Figure 5, from 70 percent speed to 100 percent speed, collapsed into a single curve, even though

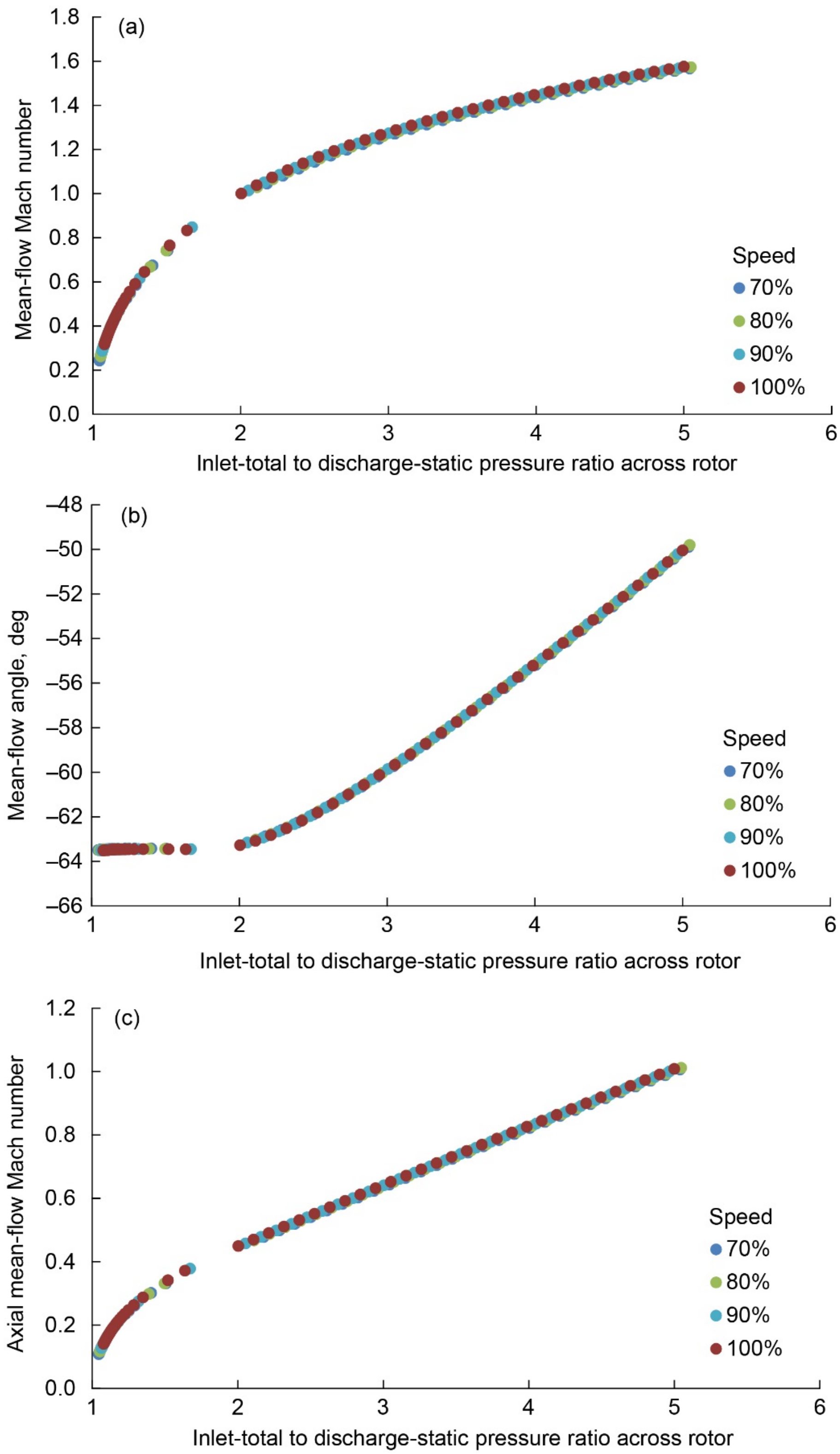

Figure 5.—NASA/P&W lift-fan turbine. Mean-flow properties at last rotor discharge. (a) Mean-flow Mach number. (b) Mean-flow angle. (c) Axial component of mean-flow Mach number.

Figures 2, 3, and 4 have clearly shown that the performance-characteristics, such as efficiency, mass-flow-rate, and torque-production, have quite different behavioral characteristics at different speed-lines. This is just an interesting observation, no particular explanation is offered here, except that one can state with certainty that the calculations were sound.

The torque produced by the last rotor alone (rotor-4 of Ref. 4), post-processed from AXOD2-result isolating the last rotor, is shown by Figure 6. The abscissa is the same as that of Figure 5. AXOD2-simulations were terminated at the formal limit-loading condition of Equation (30).

Shown in Figure 6, different speed-of-rotation clearly possessed different torque-production. The peak-of-torque, and the drop-down in trending after the peak can be seen at every speed-line, although not as clear as that shown in Figure 4 (the overall-torque plots). The reason is because the abscissa here is the total-to-static pressure ratio across the last rotor, while in Figure 4 the abscissa was the overall total-to-total pressure ratio across the turbine assembly. There is a scale-factor between the two abscissas, and the plots of Figure 4 were more packed-in than plots of Figure 6 shown here. The point of maximum-torque occurred on the data-series is marked by a diamond-shape symbol in Figure 6 for easier visual identification.

Again, the presence of a peak, and the drop-down in torque-production were not observed in the CFD-investigation in Part-1 of the paper (Fig. 5 of Ref. 1). And as argued before, this behavior (the peak, and the downward-trend after the peak) is an anomaly from the one-dimensional model-treatment of the supercritical flow of AXOD2. The correct physical behavior is believed to be that the torque should be saturating into a constant-trend, and never would decrease at any given pressure ratio, as that have shown by Figure 5 of Reference 1.

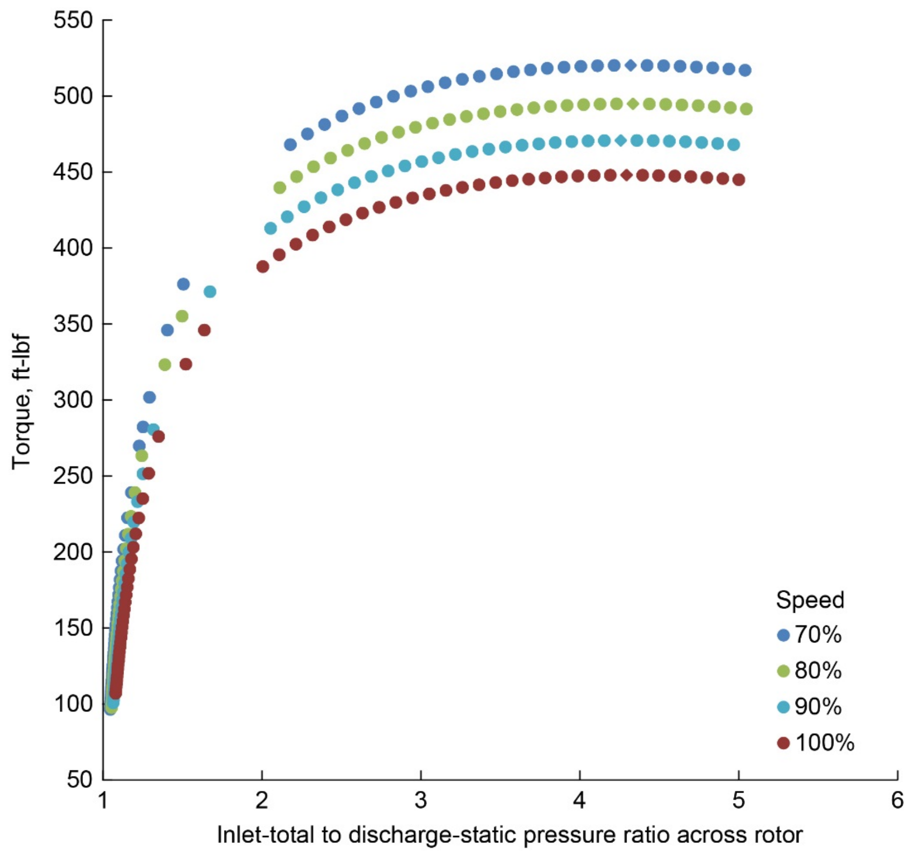

Figure 6.—NASA/P&W lift-fan turbine. Torque produced by the last rotor.

4.2 NASA Three and One-Half (3 ½)-Stage Fan-Drive Turbine

This case was also studied and presented in the previous publication of Reference 8, but with only results from 70 and 100 percent speed-lines. Here 70, 80, 90, and 100 percent speeds were investigated. The process and procedure of the AXOD2 simulation were exactly the same as that described in Reference 8. The same optimum loss-coefficients were applied in this work. Five sectors were given radially for the flow passage. The result-comparisons of the overall total efficiency, equivalent mass-flow-rate, and the overall equivalent-torque produced are presented in Figure 7, Figure 8, and Figure 9, respectively. The abscissa is the overall total (absolute) -to- total (absolute) pressure ratio across the turbine stages. Experimental data were published in Reference 5.

The solid red-block at 100 percent speed-line in Figure 7 is the design-point identified by the experiment. The experimental data plotted here were scanned and digitized directly from plots (of the 3 1/2-stage) in Reference 5.

The match between the AXOD2-results and the experimental data were good, but not as impressive as the previous example (Section 4.1). The reason may be because in this case, the kinetic energy loss-coefficient (the Y_B of Eq. (4)) in the rotors were assigned twice as high in-proportion to that of the stators, while in the previous-case of Section 4.1, the kinetic energy loss in the rotors and the stators were set equal in proportionality. The higher loss in the rotors may have been less accurate physically, and that may have caused the trending predicted by AXOD2 to be off, greater than the previous case-study. From our experience, the loss-factors do have noticeable effect on the predicted outcome, specifically, the trending at far off-design. Random assignment of the loss-factors would be unacceptable. The similarity laws (the proportionalities of the blade-row losses, or simply put, the loss-correlations) and the loss-model closure technique introduced in Reference 7 are quite satisfactory and reliable. They should be followed with confidence as the standard in problem solving. Care should be taken, however, when

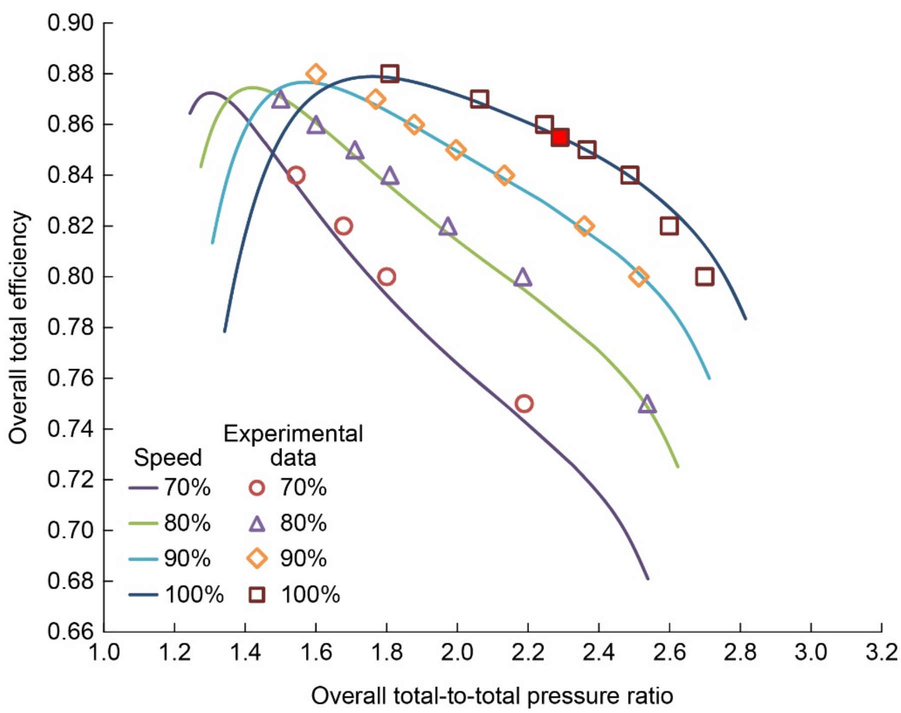

Figure 7.—NASA (3½)-stage fan-drive turbine. Comparison of overall total efficiency between AXOD2 simulation-result and experimental data of Reference 5.

multiplying ‘extra loss factors’ to the baseline similarity laws, since the extra-loss-factors structured in AXOD2 are strictly user-given quantities. There should be a justifiable reason for the compensation of an extra blade-row loss (e.g., coolant-flow injection, or tip-clearance leakage loss, etc.). If the compensation via the venue of extra-loss allocated in the code is physically justifiable, then it should enhance the performance-prediction of AXOD2, both locally sector-by-sector and in the overall sense, stage-by-stage. If the extra-loss is applied just by intuition alone, the outcome (trending) could be realistically worse than not applying the extra-loss (no compensation) at all. This has been tested and confirmed to be true. When lacking of information for a justifiable compensation, doing without it would be a safe and viable option. The reason is that the proportionality relation of the built-in loss-correlations are capable of absorbing the difference evenly into the proportionality constants, which are to be determined through the matching process of the loss-model closure technique. The trending of the overall performance would likely remain to be physically trackable and realistic. The sector behavior, however, could be questionable in that regards.

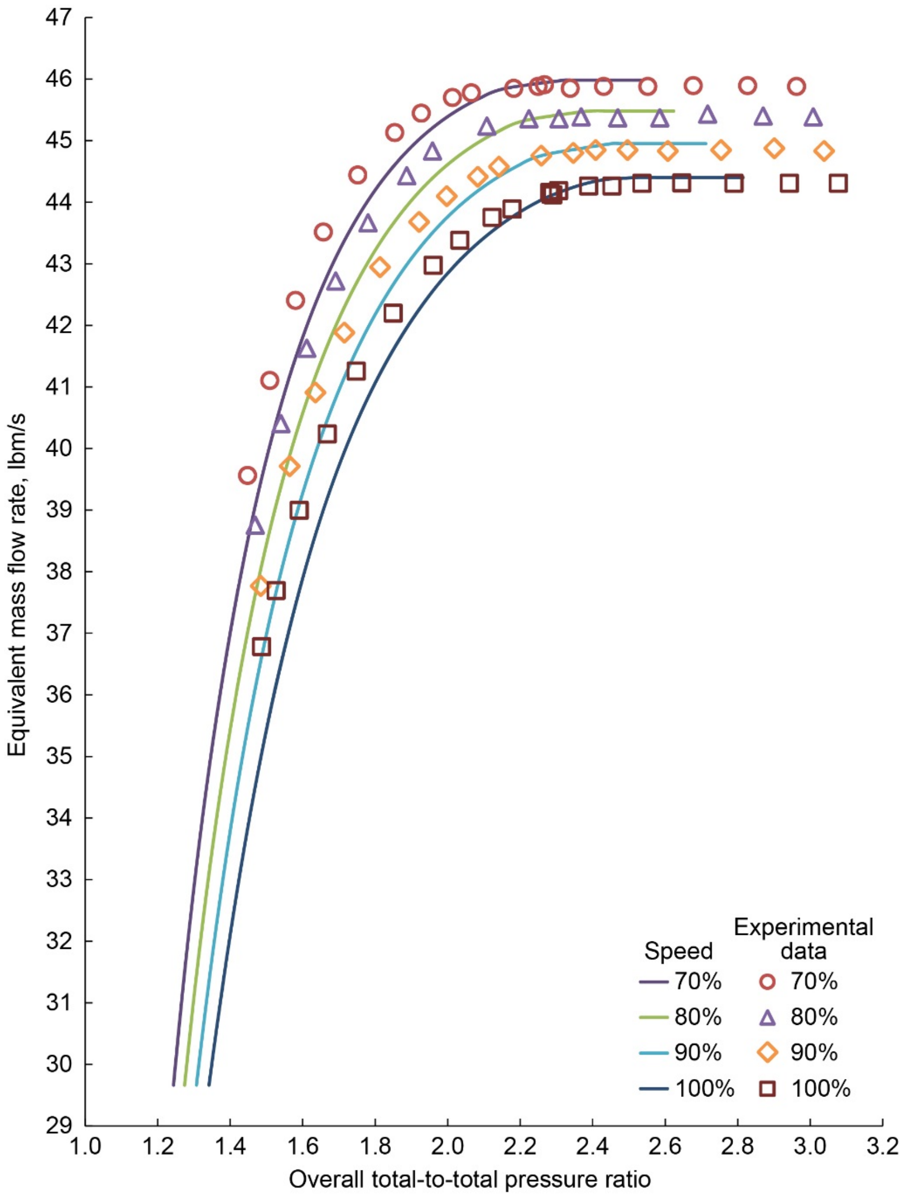

Figure 8.—NASA (3½)-stage fan-drive turbine. Comparison of equivalent mass flow rate between AXOD2 simulation-result and experimental data of Reference 5.

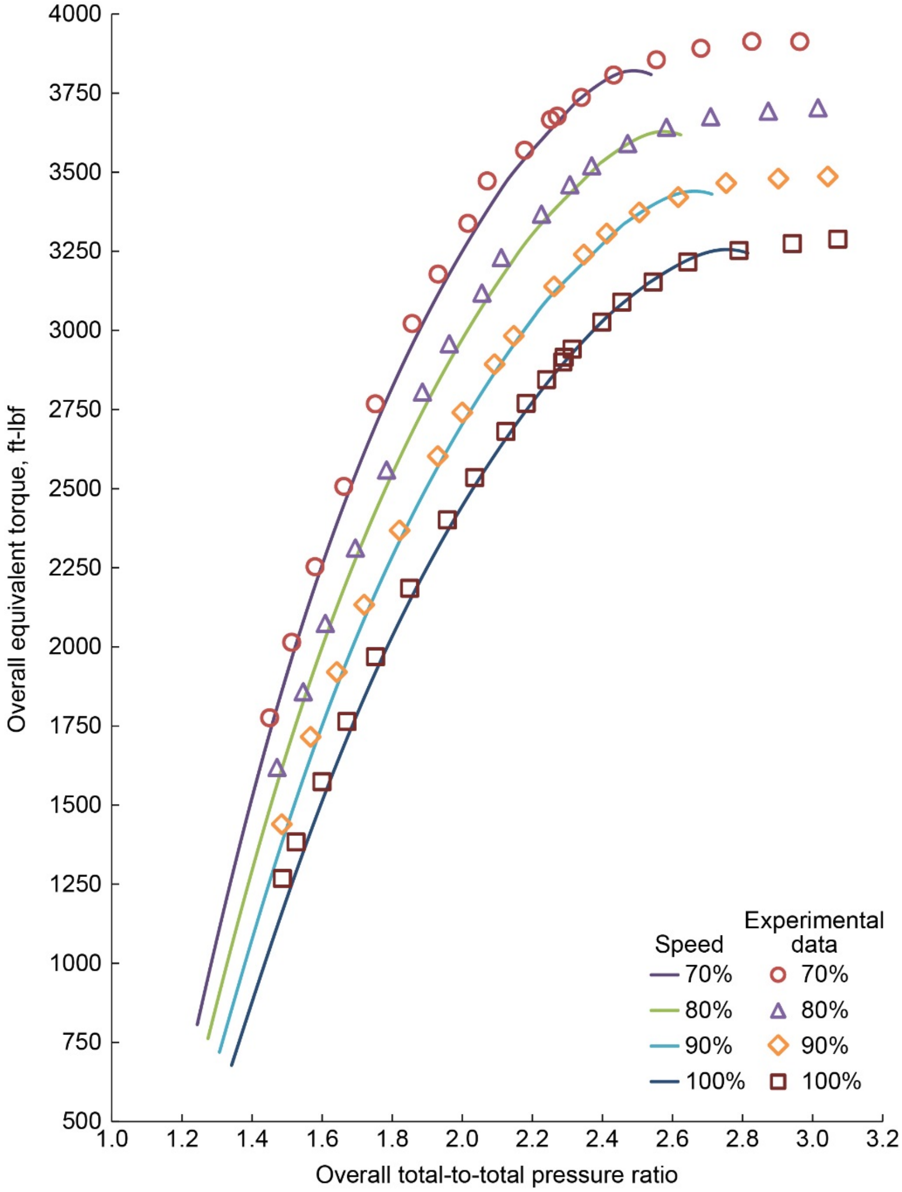

Figure 9.—NASA (3½)-stage fan-drive turbine. Comparison of overall equivalent-torque between AXOD2 simulation-result and experimental data of Reference 5.

The mass-averaged mean-flow properties over the three-dimensional blade-row outlet of the last rotor (rotor-3 of Ref. 5), defined and calculated according to Equations (35) to (37), are shown here by Figure 10. These results are to be compared with results of the CFD-investigation shown by Figure 3 of Reference 1, and to compare with Figure 5 of the previous case-study (Section 4.1). The Mach numbers and the flow angles plotted here are flow-quantities of the relative (rotational) frame-of-reference, since they are the results of a rotor blade-row recorded in AXOD2. The abscissa in Figure 10 is the mass-averaged inlet-total (relative) to discharge-static (actual) pressure ratio across the last rotor.

The comments are the same as discussed before in Figure 5 of the previous case-study (Section 4.1).

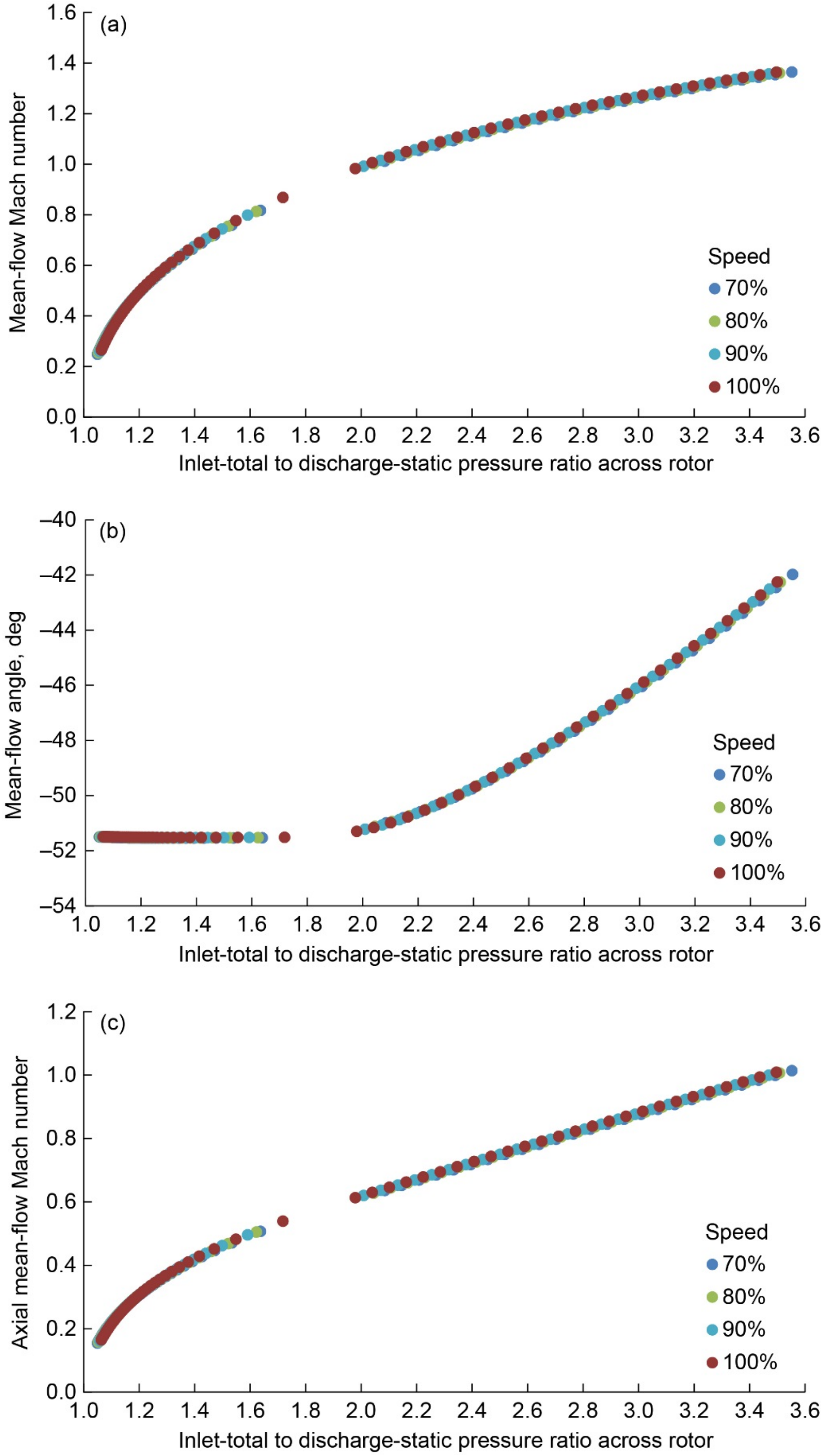

Figure 10.—NASA fan-drive turbine. Mean-flow properties at last rotor discharge. (a) Mean-flow Mach number. (b) Mean-flow angle. (c) Axial component of mean-flow Mach number.

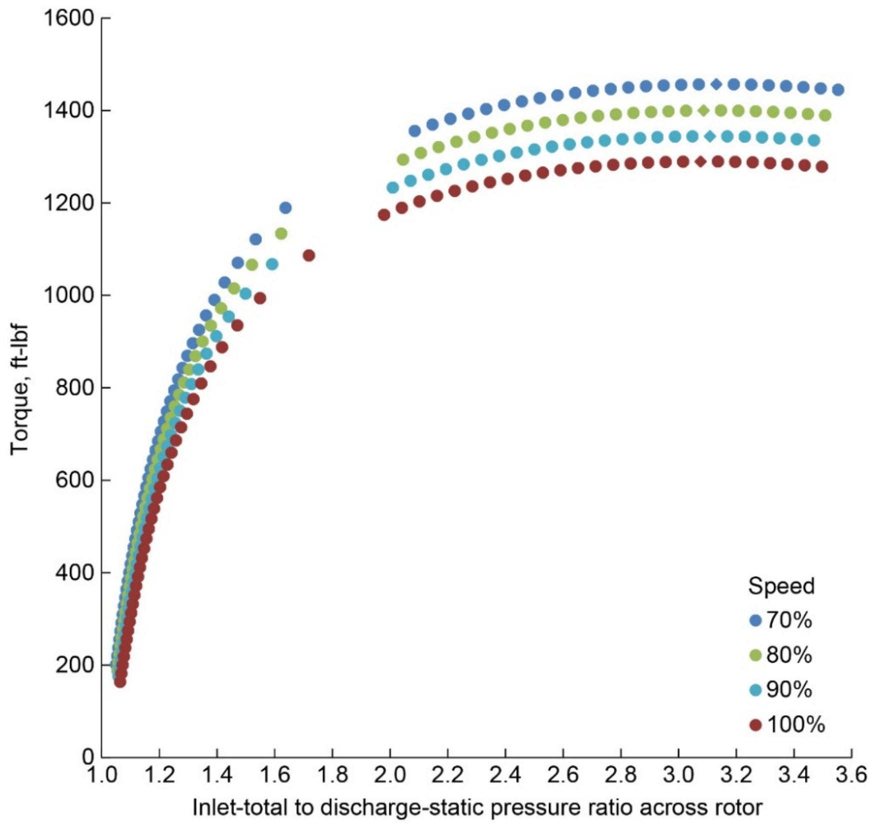

Figure 11.—NASA fan-drive turbine. Torque produced by the last rotor.

Lastly, the torque produced by the last rotor (rotor-3 of Ref. 5) is shown by Figure 11. The abscissa is the same as that of Figure 10. AXOD2-simulations stopped at the formal limit-loading condition of Equation (30). The diamond-shape symbol in Figure 11 marks the point of maximum-torque occurred on the data-series.

The comments are the same as those discussed in Figure 6 of the previous case-study (Section 4.1).

5.0 Concluding Remarks

The supercritical flow modeling approach and model treatment applied in AXOD2 is simple yet intriguing. The bases of this flow-treatment are highly analytical and followed the mathematical principles and the laws of gas dynamics rigorously. It is a one-dimensional modeling approach, but it captures the salient physical characteristics of the supercritical-flow in axial-flow turbines. This flow-treatment was described in this paper thoroughly, together with step-by-step derivation of the mathematical equations and conditions involved. The intention was to write these down clearly and to keep them as a form of documentation for future reference, since they have not been revealed as completely before. This paper might have served that purpose.

The performance of this one-dimensional modeling approach for supercritical-flow was compared head-to-head with experimental data from two published case-studies obtained in a rotating turbine rig, and with results of the two-dimensional CFD-investigation presented in the Part-1 of the paper. The success and shortfall of the supercritical flow model-treatment of AXOD2 were illustrated and addressed in this paper.

The results of AXOD2-prediction compared favorably with the experimental data, however, the one-dimensional modeling concept for supercritical-flow broke down in region near and beyond the formal limit-loading condition. That is the limitation of the model treatment for supercritical-flow currently implemented in AXOD2. In all, the performance of AXOD2 was impressive.

Appendix A.—Mathematical Relation of Ideal Total Pressure (Pt^{ideal}) and Ideal Total Temperature (Tt^{ideal}) With Respect to Isentropic Total Temperature (Tt^{isen}) and the Actual Flow Quantities

The ideal total pressure is defined as the total pressure at the end-state of an isentropic process, where the path of this process passes through a known point-of-state. The relation of this is a basic law of thermodynamics, it can be expressed in form of total-to-total flow properties along the isentropic path. The formula provided here is available in textbooks of fundamental (classic) thermodynamics.

For clarity, we shall cast equations of the stator and equations of the rotor in separate forms.

In mathematical form of the present application, this isentropic relation can be written as:

$$\left(Pt_1^{ideal}\right) = \left[Pt_{0,1}\left(\frac{Tt_1{}^{isen}}{Tt_{0,1}}\right)^{\frac{\gamma}{\gamma-1}}\right] \tag{A.1S}$$

$$(Pt')_2^{ideal} = \left[(Pt')_{1A,2}\left(\frac{(Tt'_2)^{isen}}{(Tt')_{1A,2}}\right)^{\frac{\gamma}{\gamma-1}}\right] \tag{A.1R}$$

Equation (A.1S) is for the stator, subscripts ‘0’ represents the stator inlet-state, ‘1’ represents the stator discharge-state, ‘0,1’ represents an interim state immediate after state ‘0’ (see Ref. 2 for definition of the interim state).

Equation (A.1R) is for the rotor, subscripts ‘1A’ represents the rotor inlet-state, ‘2’ represents the rotor discharge-state, ‘1A,2’ represents the interim state immediate after state ‘1A’ (again, see Ref. 2 for definition of this interim state). The superscript ‘prime’ denotes flow-quantity of the relative (rotational) frame-of-reference.

The known point-of-state in (A.1S) is the state ‘0,1’, the end-state is the state ‘1’. Equation (A.1S) means ($Pt_1^{ideal}, Tt_1{}^{isen}$) are the *isentropic* total pressure and total temperature at state ‘1’, where the flow varied isentropically from the *actual* total pressure and total temperature ($Pt_{0,1}$ and $Tt_{0,1}$) at state ‘0,1’ to the state of ‘1’.

Similarly, the known point-of-state in (A.1R) is the state ‘1A,2’, the end-state is the state ‘2’. Equation (A.1R) means ($(Pt')_2^{ideal}$, $(Tt'_2)^{isen}$) are the *isentropic* total pressure and total temperature at state ‘2’, where the flow varied isentropically from the *actual* total pressure and total temperature ($Pt'_{1A,2}$ and $Tt'_{1A,2}$) at state ‘1A,2’ to the state of ‘2’. Again, superscript ‘prime’ denotes relative flow-quantity.

Now, although there is flow-momentum loss (total-pressure loss) at the inlet stagnation region (see Refs. 2, 7 for full description), but the flow-process from the state-of-inlet to the interim-state can be assumed without appreciable external heat-exchange or heat-input, and without appreciable difference in blade-velocities. Thus, the total enthalpy (of both the absolute-frame and the relative-frame) would remain un-changed in this process. I.e.,

$$Tt_0 = Tt_{0,1} \tag{A.2S}$$

$$(Tt')_{1A} = (Tt')_{1A,2} \tag{A.2R}$$

These relationships can be derived from the energy-balance equations, Equations (A.4S) and (A.4R), shown later.

Put (A.2S), (A.2R) into Equations (A.1S) and (A.1R); divide P_1 to both side of (A.1S), divide P_2 to both side of (A.1R), we get:

$$\left(Pt_1^{ideal}\right)\Big/_{P_1} = \left[Pt_{0,1}\left(\frac{Tt_1{}^{isen}}{Tt_0}\right)^{\frac{\gamma}{\gamma-1}}\right]\Big/_{P_1} \tag{A.3S}$$

$$(Pt')_2^{ideal}\Big/_{P_2} = \left[(Pt')_{1A,2}\left(\frac{(Tt'_2)^{isen}}{(Tt')_{1A}}\right)^{\frac{\gamma}{\gamma-1}}\right]\Big/_{P_2} \tag{A.3R}$$

Equations (A.3S) and (A.3R) are Equations (6S) and (6R) given in Reference 2. However, in Reference 2 the two equations were mistakenly expressed.

As seen derived, there should be a superscript 'isen' on the end-state total temperatures, as of $Tt_1{}^{isen}$ and $(Tt'_2)^{isen}$. In Reference 2, however, Tt_1 and (Tt'_2) were written instead. They are hereby formally revised.

Notice that in Equation (A.1S) (or Eq. (A.1R)), Pt^{ideal} (or $(Pt')^{ideal}$) was used instead of using the nomenclature of Pt^{isen} (or $(Pt')^{isen}$). The reason is because later on a corresponding ideal total temperature, Tt^{ideal}, will be defined. To make distinction between this ideal total temperature and the isentropic total temperature of Equation (A.1S) (or Eq. (A.1R)), we elect to use the nomenclature of Pt^{ideal} instead of using Pt^{isen} to avoid ambiguity and confusion, because Tt^{ideal} and Tt^{isen} are different thermodynamic quantities, even though Pt^{ideal} and Pt^{isen} are one.

To connect isentropic total temperature to the actual physical flow quantities, one works with the energy-balance equation.

Recapped from Reference 2, the energy equations applied to AXOD2 can be written as:

$$cp_0 \times Tt_0 + \left(w_{r_1} - 1\right) \times cp_{0-1}^{cool} \times Tt_{0-1}^{cool} = w_{r_1} \times cp_1 \times Tt_1 \tag{A.4S}$$

$$cp_{1A} \times \left[Tt'_{1A} + \left(U_2{}^2 - U_{1A}{}^2\right)\Big/_{(2GJ \times cp_{1A})}\right] + \left(w_{r_2} - 1\right) \times cp_{1A-2}^{cool} \times Tt'^{\,cool}_{1A-2} = w_{r_2} \times cp_2 \times Tt'_2 \tag{A.4R}$$

The superscript '*cool*' denotes the coolant-flow property. The $\left(w_{r_1} - 1\right)$ and $\left(w_{r_2} - 1\right)$ are the added coolant-flow mass-fraction with respect to the inlet mass-flow-rate, respectively for the stator and for the rotor. The U_2 is the tangential blade-velocity at rotor discharge, U_{1A} is the tangential blade-velocity at the rotor inlet. The 'cp' denotes specific heat at constant pressure. The two equations were given as Equation (9S) and Equation (9R-1) in Reference 2.

As seen, the energy equation applied to AXOD2 does not explicitly contain frictional energy-loss term, even though the flow in the blade-row passage is frictional (see the assumptions made in Reference 2 with this regard), however, it does include the coolant-flow addition.

The *isentropic* total temperature at the blade-row discharge station, by its definition, is the total temperature excluding the external heat-exchange (coolant-flow input) and the frictional energy-loss (if any) occurred in blade-row.

Thus, by definition, one writes the balance-equation of energy for the isentropic total temperature as:

$$cp_0 \times Tt_0 = cp_1 \times {Tt_1}^{isen} \tag{A.5S}$$

$$cp_{1A} \times \left[Tt'_{1A} + \left({U_2}^2 - {U_{1A}}^2\right) \Big/ (2GJ \times cp_{1A}) \right] = cp_2 \times (Tt'_2)^{isen} \tag{A.5R}$$

Equations (A.5S) and (A.5R) defined the *isentropic* total temperature at the blade-row discharge station, in terms of the *actual* flow-quantities and physical-properties of the blade-row. With these relations, the key quantities $\left(Pt_1^{ideal}\right) \big/ P_1$ and $(Pt')_2^{ideal} \big/ P_2$ expressed in Equations (A.3S) and (A.3R), respectively, can now be related to the actual physical- and flow- quantities, and be meaningful.

A couple of notes in regard to the isentropic total temperature: according to the energy equations, Equations (A.4S) and (A.4R) applied to AXOD2, which come with a few idealizations and assumptions of their own (provided in Ref. 2), one observes that, when without the coolant-flow addition, the *isentropic* total temperature at a blade-row discharge (shown by Eqs. (A.5S) and (A.5R)) would be identical to the *actual* total temperature there; however, when there is coolant-flow addition, the *isentropic* total temperature at the blade-row discharge would be quite different from the *actual* total temperature, by virtue of the heat-and-mass addition brought-in with the coolant-flow injection.

If the coefficients of specific heat at constant pressure, (cp_0, cp_1) and (cp_{1A}, cp_2), were averaged between their corresponding starting-state and ending-state. I.e., when considered

$$cp_0 \sim cp_1 \sim \overline{cp_{stator}}$$

$$cp_{1A} \sim cp_2 \sim \overline{cp_{rotor}}$$

Equations (A.5S) and (A.5R) can be written into the simplified forms of

$$Tt_0 = {Tt_1}^{isen} \tag{A.6S}$$

$$\left[Tt'_{1A} + \left({U_2}^2 - {U_{1A}}^2\right) \Big/ \left(2GJ \times \overline{cp_{rotor}}\right) \right] = (Tt'_2)^{isen} \tag{A.6R}$$

Equations (A.6S) and (A.6R) are the forms-of-relation of the isentropic total temperature with respect to the known actual quantities, that were applied (implemented) in the coding of AXOD2/AXOD (Refs. 2 and 3). Specifically, they were applied to Equations (A.3S) and (A.3R).

Lastly, the ideal total temperature is defined in correspondence to the ideal total pressure as:

$$\left(Tt_1^{ideal} \big/ T_1 \right) = \left(Pt_1^{ideal} \big/ P_1 \right)^{\frac{\gamma-1}{\gamma}}$$

$$\left((Tt')_2^{ideal} \big/ T_2 \right) = \left((Pt')_2^{ideal} \big/ P_2 \right)^{\frac{\gamma-1}{\gamma}}$$

Noted here, Tt^{ideal} is an idealized total temperature at the end-state of ‘1’ or ‘2’, where the flow is brought to zero velocity locally via the isentropic-condition. Whereas Tt^{isen}, seen in Equation (A.5S) or Equation (A.5R), is the isentropic total temperature, brought to the end-state from the known state of ‘0’ (or ‘1A’) via an isentropic flow-process.

Thus, Tt^{ideal} and Tt^{isen} are two entirely different thermodynamic quantities. They generally do not possess the same number-value in a real flow.

This has completed the derivations for the basic laws of thermodynamics and gas-dynamics applied in AXOD2.

Appendix B.—Derivation for Critical Condition of Mass Flow Function

Recap the relevant equations:
The non-isentropic mass flow function is

$$\left(\frac{\omega}{A}\right)\frac{\sqrt{Tt_1}}{Pt_1^{ideal}} = \sqrt{\frac{2\gamma G}{(\gamma-1)R}}\left(\eta_B\left(1-\frac{1}{\phi}\right)\right)^{\frac{1}{2}} \times \frac{1}{\left(1-\eta_B\left(1-\frac{1}{\phi}\right)\right)} \times \left(\frac{1}{\phi^{\frac{\gamma}{\gamma-1}}}\right) \tag{B.1}$$

Let

$$\psi = \left.\left(\frac{\omega}{A}\right)\frac{\sqrt{Tt_1}}{Pt_1^{ideal}}\right/\sqrt{\frac{2\gamma G}{(\gamma-1)R}}$$

and let

$$X = \eta_B\left(1-\frac{1}{\phi}\right) \tag{B.2}$$

Equation (B.1) can now be written in the form of

$$\psi = X^{\frac{1}{2}}\,\frac{1}{(1-X)}\,\frac{1}{\left(\frac{\eta_B}{\eta_B-X}\right)^{\frac{\gamma}{\gamma-1}}} \tag{B.3}$$

As stated in the main text, the critical-point lies at when

$$\frac{d\psi}{dX} = 0 \tag{B.4}$$

Differentiate ψ of Equation (B.3) with respect to X, one gets

$$\begin{aligned} 0 = \frac{d\psi}{dX} = \frac{1}{2}\,X^{-1/2}\,(1-X)^{-1}\left(\frac{\eta_B}{\eta_B-X}\right)^{\frac{-\gamma}{\gamma-1}} + X^{1/2}\,(1-X)^{2}\left(\frac{\eta_B}{\eta_B-X}\right)^{\frac{-\gamma}{\gamma-1}} \\ -X^{1/2}\,(1-X)^{-1}\left(\frac{\gamma}{\gamma-1}\right)(\eta_B-X)^{-1}\left(\frac{\eta_B}{\eta_B-X}\right)^{\frac{-\gamma}{\gamma-1}} \end{aligned} \tag{B.5}$$

Multiply $\left[X^{1/2}\,(1-X)^2\,(\eta_B-X)\right]$ to both side, and take-out the common factor $\left(\frac{\eta_B}{\eta_B-X}\right)^{\frac{-\gamma}{\gamma-1}}$ in Equation (B.5), we get

$$0 = \frac{1}{2}\,(1-X)\,(\eta_B-X) + X\,(\eta_B-X) - \left(\frac{\gamma}{\gamma-1}\right)X\,(1-X) \tag{B.6}$$

Rearrange Equation (B.6) into quadratic form, we have

$$0 = \left(-\frac{1}{2}+\frac{\gamma}{\gamma-1}\right)X^2 + \left(\frac{\eta_B-1}{2}-\frac{\gamma}{\gamma-1}\right)X + \frac{\eta_B}{2} \tag{B.7}$$

Solution of Equation (B.7) will be at

$$X_{critical} = {\left[-B \pm \sqrt{B^2 - 4AC}\right]}\Big/{(2A)} \tag{B.8}$$

with

$$A = \left(\frac{\gamma}{\gamma - 1}\right) - \frac{1}{2}$$
$$B = -\left[\left(\frac{\gamma}{\gamma - 1}\right) + \frac{1 - \eta_B}{2}\right]$$
$$C = \frac{\eta_B}{2}$$

In Equation (B.8), the solution with the + sign, i.e., $X = {\left[-B + \sqrt{B^2 - 4AC}\right]}\Big/{(2A)}$ leads to the result of $X > 1$. From Equation (B.2), one has

$$\phi_{critical} = \frac{\eta_B}{\eta_B - X}$$

A solution with $X > 1$ would result in a negative $\phi_{critical}$ since η_B is less than 1.0. Which means the solution of ϕ so obtained is non-physical and thus unacceptable.

Thus, one concludes, the correct solution of Equation (B.4) lies at

$$X_{critical} = {\left[-B - \sqrt{B^2 - 4AC}\right]}\Big/{(2A)} \tag{B.8}$$

with

$$A = \left(\frac{\gamma}{\gamma-1}\right) - \frac{1}{2} \tag{B.9}$$
$$B = -\left[\left(\frac{\gamma}{\gamma-1}\right) + \frac{1-\eta_B}{2}\right] \tag{B.10}$$
$$C = \frac{\eta_B}{2} \tag{B.11}$$

Equation (B.8), together with Equations (B.9), (B.10), and (B.11) were the result given in the main text as Equation (17).

Some simple check-up (with $\gamma = 1.4$):

1. When $\eta_B = 1$, we have $X_{critical} = 0.1667$, and thus $\phi_{critical} = 1.2$. From Equation (19) of the main text, we know $\phi_{critical} = \left(\frac{Tt_1^{ideal}}{T_{critical}}\right)$. The value of $\left(\frac{Tt_1^{ideal}}{T_{critical}}\right) = 1.2$ is the theoretical value for isentropic flow, seen cited in the literature. The corresponding $\left(\frac{Pt_1^{ideal}}{P_{critical}}\right)$, which by definition equals $(\phi_{critical})^{\frac{\gamma}{\gamma-1}}$, is 1.8929, which also is the theoretical value for isentropic flow.
2. When $\eta_B = 0.9$, we have $X_{critical} = 0.1444$, and thus $\phi_{critical} = 1.191$. And we know $\phi_{critical} = \left(\frac{Tt_1^{ideal}}{T_{critical}}\right)$. A value of $\left(\frac{Tt_1^{ideal}}{T_{critical}}\right) = 1.191$ is reasonable for a real flow. The corresponding $\left(\frac{Pt_1^{ideal}}{P_{critical}}\right)$, which equals $(\phi_{critical})^{\frac{\gamma}{\gamma-1}}$, will be 1.844, which would also be reasonable as a real flow.

References

1. Chen, S.S.: Axial-Flow Turbine Rotor Discharge-Flow Overexpansion and Limit-Loading Condition. Part 1: Computational Fluid Dynamics (CFD) Investigation. NASA/TM—2017-219506, July 2017.
2. Chen, S.S.: A Guide to Axial-Flow Turbine Off-Design Computer Program AXOD2. NASA/TM—2014-218301, June 2014.
3. Glassman, A.J.: Modeling Improvements and Users Manual for Axial-Flow Turbine Off-Design Computer Code AXOD. NASA CR 195370, August 1994.
4. Whitney, W.J., Behning, F.P., Moffitt, T.P., and Hotz, G.M.: Cold-Air Investigation of $4\frac{1}{2}$-Stage Turbine with Stage Loading Factor of 4.66 and High Specific Work Output. I-Overall Performance. NASA TM X-3498, February 1977.
5. Whitney, W.J., Schum, H.J., and Behning, F.P.: Cold-Air Investigation of a $3\frac{1}{2}$-Stage Fan-Drive Turbine with a Stage Loading Factor of 4 Designed for an Integral Lift Engine. II-Performance of 2-, 3-, and $3\frac{1}{2}$-Stage Configurations. NASA TM X-3482, February 1977.
6. Flagg, E.E.: Analytical Procedure and Computer Program for Determining the Off-Design Performance of Axial Flow Turbines. NASA CR-710, February 1967.
7. Chen, S.S.: Preliminary Axial Flow Turbine Design and Off-Design Performance Analysis Methods for Rotary Wing Aircraft Engines. I-Validation. NASA/TM—2009-215651/PART1, May 2009.
8. Chen, S.S.: Capability Extension to the Turbine Off-Design Computer Program AXOD With Applications to the Highly Loaded Fan-Drive Turbines. NASA/TM—2011-217129, July 2011.
9. Shapiro, A.H.: Compressible Fluid Flow. vol. 1. John Wiley & Sons, Inc., New York, NY, 1953.
10. Glassman, A.J., ed.: Turbine Design and Application. Volume 1. NASA SP-290, 1972.